Cell Reports

Article

Development of sexual dimorphism of skeletal muscles through the adrenal cortex, caused by androgen-induced global gene suppression

Graphical abstract

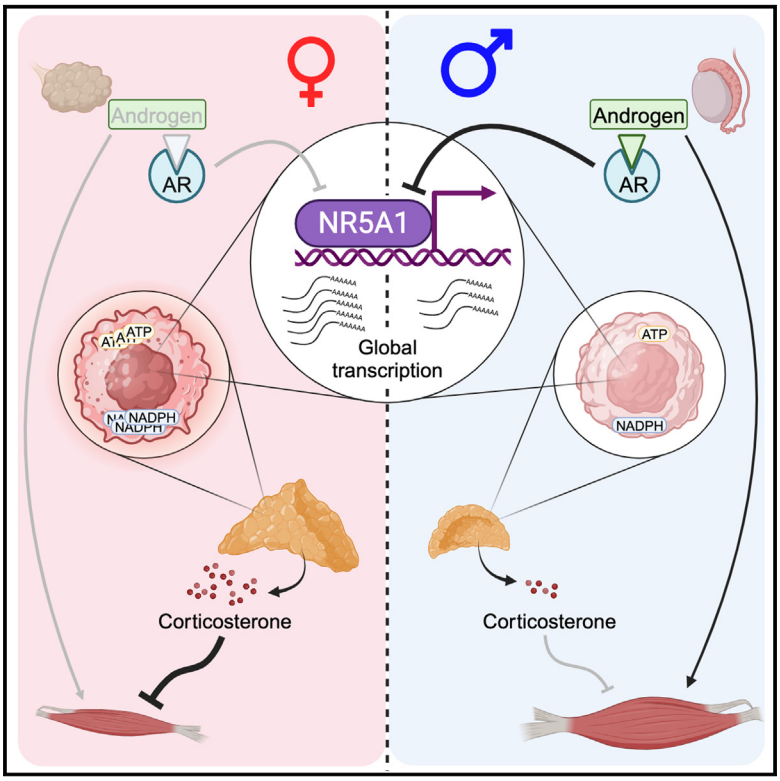

Highlights

- Adrenal zona fasciculata cells show globally female-biased transcription
- *Nr5a1* governs gene expression globally in adrenal zona fasciculata cells
- Androgen suppresses cellular transcription globally via suppressing *Nr5a1*
- Sexually dimorphic corticosterone levels trigger sex difference in skeletal muscles

Authors

Fumiya Takahashi, Takashi Baba, Antonius Christianto, ..., Takehiko Yokomizo, Man Ho Choi, Ken-ichirou Morohashi

Correspondence

baba.takashi.547@m.kyushu-u.ac.jp (T.B.), morohashi.ken-ichirou.874@m.kyushu-u.ac.jp (K.-i.M.)

In brief

Takahashi et al. demonstrate globally female-biased transcription impacting glucocorticoid synthesis in adrenocortical zona fasciculata cells. NR5A1 (Ad4BP/SF-1) possibly mediates androgen-induced suppression of global transcription. This study suggests a pathway for sex differentiation via glucocorticoid synthesis, affecting various tissues due to the ubiquitous expression of glucocorticoid receptor.

Takahashi et al., 2024, Cell Reports *43*, 113715
February 27, 2024
https://doi.org/10.1016/j.celrep.2024.113715

CellPress

Cell Reports

CellPress
OPEN ACCESS

Article

Development of sexual dimorphism of skeletal muscles through the adrenal cortex, caused by androgen-induced global gene suppression

Fumiya Takahashi,[1] Takashi Baba,[1,2,*] Antonius Christianto,[1,2] Shogo Yanai,[1] Hyeon-Cheol Lee-Okada,[3] Keisuke Ishiwata,[4] Kazuhiko Nakabayashi,[4] Kenichiro Hata,[4,5] Tomohiro Ishii,[6] Tomonobu Hasegawa,[6] Takehiko Yokomizo,[3] Man Ho Choi,[7] and Ken-ichirou Morohashi[1,2,8,9,*]

[1]Department of Systems Life Sciences, Graduate School of Systems Life Sciences, Kyushu University, 3-1-1 Maidashi, Higashi-ku, Fukuoka 812-8582, Japan
[2]Department of Molecular Biology, Graduate School of Medical Sciences, Kyushu University, 3-1-1 Maidashi, Higashi-ku, Fukuoka 812-8582, Japan
[3]Department of Biochemistry, Juntendo University Graduate School of Medicine, 2-1-1 Hongo, Bunkyo-ku, Tokyo 113-8421, Japan
[4]Department of Maternal-Fetal Biology, Research Institute, National Center for Child Health and Development, 2-10-1 Okura, Setagaya-ku, Tokyo 157-0074, Japan
[5]Department of Human Molecular Genetics, Gunma University Graduate School of Medicine, Maebashi, Gunma 371-8511, Japan
[6]Department of Pediatrics, Keio University School of Medicine, 35 Shinanomachi, Shinjuku-ku, Tokyo 160-8582, Japan
[7]Center for Advanced Biomolecular Recognition, Korea Institute of Science and Technology, Seoul 02792, Korea
[8]Department of Internal Medicine, Kurume University School of Medicine, 67 Asahimachi, Kurume 830-0011, Japan
[9]Lead contact
*Correspondence: baba.takashi.547@m.kyushu-u.ac.jp (T.B.), morohashi.ken-ichirou.874@m.kyushu-u.ac.jp (K.-i.M.)
https://doi.org/10.1016/j.celrep.2024.113715

SUMMARY

The zona fasciculata (zF) in the adrenal cortex contributes to multiple physiological actions through glucocorticoid synthesis. The size, proliferation, and glucocorticoid synthesis characteristics are all female biased, and sexual dimorphism is established by androgen. In this study, transcriptomes were obtained to unveil the sex differentiation mechanism. Interestingly, both the amount of mRNA and the expressions of nearly all genes were higher in females. The expression of *Nr5a1*, which is essential for steroidogenic cell differentiation, was also female biased. Whole-genome studies demonstrated that NR5A1 regulates nearly all gene expression directly or indirectly. This suggests that androgen-induced global gene suppression is potentially mediated by NR5A1. Using *Nr5a1* heterozygous mice, whose adrenal cortex is smaller than the wild type, we demonstrated that the size of skeletal muscles is possibly regulated by glucocorticoid synthesized by zF. Taken together, considering the ubiquitous presence of glucocorticoid receptors, our findings provide a pathway for sex differentiation through glucocorticoid synthesis.

INTRODUCTION

The adrenal cortex consists of three distinct cellular zones in humans and two zones in rodents.[1–4] The largest zone, the zona fasciculata (zF), regulates a variety of metabolic processes for carbohydrates, proteins, and lipids, as well as inflammatory reactions, and others, through synthesizing glucocorticoid.[5] It is known that the adrenal gland of rodents differs in size between males and females, and castration or treatment with androgen results in an enlargement or reduction of the organ, respectively.[6] Thereafter, studies using rodents have demonstrated that in females, the number of zF cells is larger;[7,8] the sizes of nuclei, mitochondria, and endoplasmic reticulum are larger;[9] the blood concentration of corticosterone (glucocorticoid in rodents) is higher;[6,10] the amount of lipid droplets is greater;[8] and the rate of cell division is faster.[11–13] To elucidate these sexually different features of the adrenal cortex from the aspect of gene expression, RNAs prepared from the rat adrenal cortex were analyzed using microarray.[14–16] These studies succeeded in showing the sexually different gene expression that potentially causes these different functions of the adrenal cortex according to sex.

NR5A1 (Ad4BP/SF-1) was originally identified as a transcription factor to regulate the steroidogenic *CYP11A1* and *CYP11B1* genes.[17,18] Thereafter, other steroidogenic genes were shown to be the target genes of this transcription factor.[19,20] In addition to the steroidogenic gene transcription factor, it has been shown that *Nr5a1* is implicated in steroidogenic cell differentiation because the gene disruption resulted in the disappearance of the adrenal gland, testis, and ovary.[19,21,22] Although identification of all target genes for NR5A1 is required to understand functions other than the steroidogenic gene

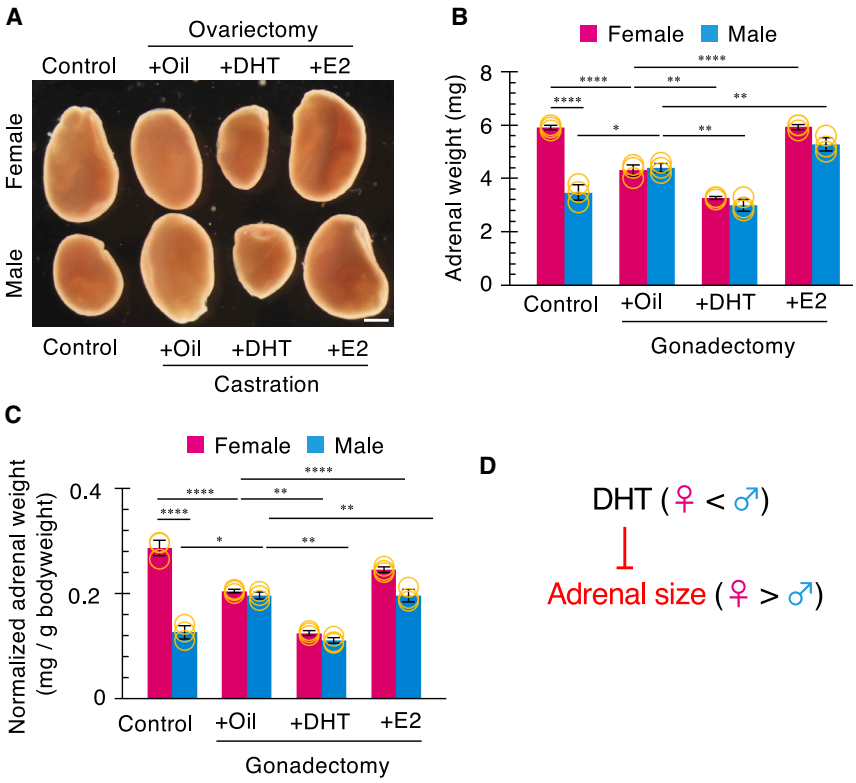

Figure 1. Adrenal size and weight are decreased by DHT

(A) Whole views of the representative adrenal glands of the eight experimental groups (sham-operated female and male [control], ovariectomized female followed by oil, DHT, or E2 treatment, and castrated male followed by oil, DHT, or E2 treatment). The scale bar represents 500 μm.

(B) Weights of adrenals.

(C) Adrenal weights normalized by body weights.

(D) Suppression of adrenal size by DHT.

Data are represented as means ± SDs (B–C). n = 3 biological replicates. *p < 0.05, **p < 0.01, ***p < 0.001, and ****p < 0.0001 by Bonferroni multiple comparison tests (B and C).

See also Figure S1.

regulator, this could not be demonstrated until an effective procedure for genome-wide study was developed.

Recently developed microarray and deep-sequencing techniques allowed us to perform these genome-wide studies and to successfully demonstrate the implications of *NR5A1/Nr5a1* in biological processes other than steroidogenesis.[23–26] These studies provided new information regarding *NR5A1/Nr5a1*'s role in heme synthesis,[24] multiple metabolic pathways such as lipid and steroid synthesis,[25] angiogenic processes,[23] glycolysis,[27] cytoskeleton remodeling,[28] nicotinamide adenine dinucleotide phosphate (NADPH) synthesis,[29] and cholesterogenesis.[30] However, these studies also found many potential target genes other than those described in these papers, and the physiological significance of the integration of many genes into a single transcription factor, NR5A1, remains controversial.

Recently, it has been reported that cells potentially upregulate or downregulate global gene expression in certain conditions. This genome-wide transcriptional regulation was observed in the processes of embryonic stem cell[31,32] and fetal germ cell differentiation,[33] tumor cell growth,[32] lymphocyte activation,[34] and renewal of adult tissue[35] through activating basal functions such as translation, metabolisms, and cell division. Such genome-wide regulation, called hypertranscription, hyperactive transcription, and transcriptional amplification, has attracted attention as a novel mechanism to alter the cellular state. Although the detailed mechanisms underlying global gene regulation are still under investigation, the implications of Myc, Yap, and the chromatin remodeler Chd1 in hypertranscription were demonstrated.[31,32,34,36]

Our present study aims to clarify the mechanism for adrenocortical sex differentiation. Interestingly, we found that the amount of mRNA per adrenocortical zF cell is greater in females than in males and that nearly all gene expression is higher in females than in males. This female-elevated (male-suppressed) global gene expression was possibly achieved by *Nr5a1* gene expression suppressed by the androgen signal in males. To demonstrate the physiological significance of the sexually differentiated adrenal cortex, we showed that different sizes of skeletal muscles, according to sex, are achieved by female-biased glucocorticoid synthesis.

RESULTS

Adrenal size and weight are decreased by DHT

It is known that the size and weight of the adrenal gland of rodents are smaller in males than in females.[6] In general, sex steroids play a crucial role in establishing sex-based differences in many cell types. Therefore, we examined whether the sex steroid treatments lead to changes in adrenal size and weight. As shown in Figure 1A, the adrenal gland of the control (sham-operated) male was smaller than that of the control female at 8 weeks after birth. As shown in Figure S1A, there was no significant sex difference in adrenal gland weight in 3-week-old mice, and the sexual dimorphism became apparent thereafter, suggesting that sex steroids secreted after 3 weeks of age are responsible for the sex difference. Therefore, gonadectomy was performed at the age of 3 weeks in this study. Two weeks after the gonadectomy, 5α-dihydrotestosterone (DHT) was injected daily to mimic intrinsic continuous secretion of testosterone, while estradiol (E2) was administered every 4 days to mimic its periodic secretion (Figure S1B–S1D). Castration enlarged the male adrenal gland, and ovariectomy decreased the female adrenal gland. Consistently, administration of DHT and E2 to gonadectomized mice decreased and increased, respectively, the size and weight of the adrenal glands (Figures 1B–1D). The changes induced in the mice of the eight experimental groups described above

indicate that the sex steroids are responsible for generating sexual dimorphism in the adrenal glands.

Transcription of zF cells is globally suppressed by DHT

The adrenal cortex of postnatal mice comprises three different cellular zones: mineralocorticoid-producing zona glomerulosa (zG) cells, glucocorticoid-producing zF, and a transient fetal zone (X-zone) that presents only for a limited period after birth.[37,38] Among these cellular zones, the larger adrenal gland in females is predominantly attributable to the larger number of zF cells.[7,8] Consistently, the female zF cells were shown to be more active for cell proliferation than male cells.[11–13]

To elucidate the mechanism to establish these sex differences, we attempted to compare gene expression in zF cells between males and females. As described in the STAR Methods, zF cells were purified from *Ad4BP-BAC-EGFP* transgenic mice, whose adrenocortical cells are labeled with EGFP (Figure S2A). As shown in Figures S2B and S2C, the zF cells were successfully prepared without any contamination of the zG, X-zone, or adrenal medulla cells. Using the zF cells, we then prepared total RNA and mRNA. Since serum E2 concentration cyclically varied during every estrus cycle, mice at diestrus, when E2 concentration is lower than other stages, were used as the female control. Female mice at diestrus were prepared by pregnant mare serum gonadotropin/human chorionic gonadotropin treatment that did not influence gene expressions in the zF cells (Figures S2D and S2E; Tables S1 and S2). To our surprise, the amounts of total RNA and mRNA in female zF cells normalized by the amounts of genomic DNAs were 1.85- and 1.82-fold more than those in male cells, respectively (Figure 2A). Importantly, such sexually dimorphic amounts of RNAs could not be recovered from the adrenal medulla (Figure S2F).

Considering the differential amounts of mRNA contained in the zF cells between the two sexes, we obtained transcriptomes using cell-number-normalized RNA sequencing (CNN RNA-seq),[33] in which mRNAs prepared from the same number of zF cells (10^4 cells) of the eight experimental groups were utilized (Figure S1B). Transcriptomes of a quality sufficient for the following analyses were obtained (Tables S1 and S2). We identified 7,200 and 7,007 genes as the expressed genes in female and male zF cells, respectively, and these genes were examined in the following studies.

As shown in Figure 2B, the expression of genes was likely to be globally downregulated in male zF cells (or upregulated in female cells). Interestingly, this plot indicates that the global set of genes, rather than specific sets, undergoes upregulation in females or downregulation in males. The female gene expression was 1.86-fold higher than that of males (Figures 2C and S2G). Castration (+oil) increased the expression levels by 1.27-fold, while ovariectomy (+oil) did not seem to have any significant effect. DHT treatment after gonadectomy decreased the expression in both sexes to the level of the male. E2 treatment after castration of males increased the gene expression, whereas treatment after ovariectomy in females did not significantly increase it.

Considering the differential effects of steroids, we decided to focus our attention on the role of androgen. Male mice were treated with flutamide, an antagonist for androgen, and then the gene expression of the zF cells was examined (Figure S2H; Table S1). The inhibition of androgen signaling gradually increased gene expression, and the expression level reached a level similar to the female control after 10 days of treatment (Figures 2D; Table S2). Moreover, the gene expression of the cells treated with flutamide for 10 days resembled that of females (Figure 2E).

To investigate whether the global downregulation of gene expression by androgen occurs at the level of transcription, we performed a nascent RNA synthesis assay.[33] As shown in Figure 2F, DHT treatment in females after ovariectomy decreased nascent RNA synthesis as compared to what was seen in ovariectomized or control females. The synthesis increased in males after castration and then decreased to the comparable level of control males by DHT administration (Figure 2G).

We assumed that, together with the size and weight of the adrenal glands decreased by DHT, androgen is a key molecule in promoting sexually dimorphic gene expression in zF cells through suppression of global gene transcription (Figure 2H).

Energy metabolism is more active in female than male zF cells

As aforementioned, the amount of mRNA in a female zF cell is 1.82-fold more than that in a male cell. Therefore, we selected 2,451 genes whose expression in females is higher than in males by more than 1.82-fold. These genes were subjected to KEGG pathway analysis to uncover biological processes correlated to the female-biased genes. As shown in Figure 3A, processes related to energy metabolism such as "oxidative phosphorylation (OXPHOS)," "valine, leucine, and isoleucine degradation," "tricarboxylic acid (TCA) cycle," "fatty acid degradation (fatty acid metabolism)," and "glycolysis/gluconeogenesis" were listed with low p values. In addition to energy metabolism, the biological process "cortisol synthesis and secretion" is also noted. The expression of these genes in the eight experimental groups is shown as a heatmap (Figure 3B). All of the gene expressions are clearly synchronized; the expressions in females are greater than in males, and the expressions are increased by castration. Consistent with this, the expressions are suppressed in both sexes by treatment with DHT.

Considering that the gene expression was globally upregulated in females, it could be assumed that all biological/metabolic processes in zF cells are more active in females than in males, and our claim that not all but certain metabolic pathways are female biased might be criticized. Therefore, we selected genes whose expression is higher in males than in females and genes whose expression is less than 1.25 times higher in females. These genes were then subjected to KEGG pathway analysis. This analysis listed "MAPK signaling pathway," "C-type lectin receptor signaling pathway," and so on, as the biological processes related to the genes (Figure 3C). The expression profiles of the genes involved in these processes were investigated in the eight experimental groups. As expected, the heatmap was largely different from that of the genes involved in the energy metabolic processes (Figure 3D).

Considering the female-biased metabolic gene expression, we examined whether the energy metabolic activities of zF cells differed between the two sexes. As indicated in Figures 3E and

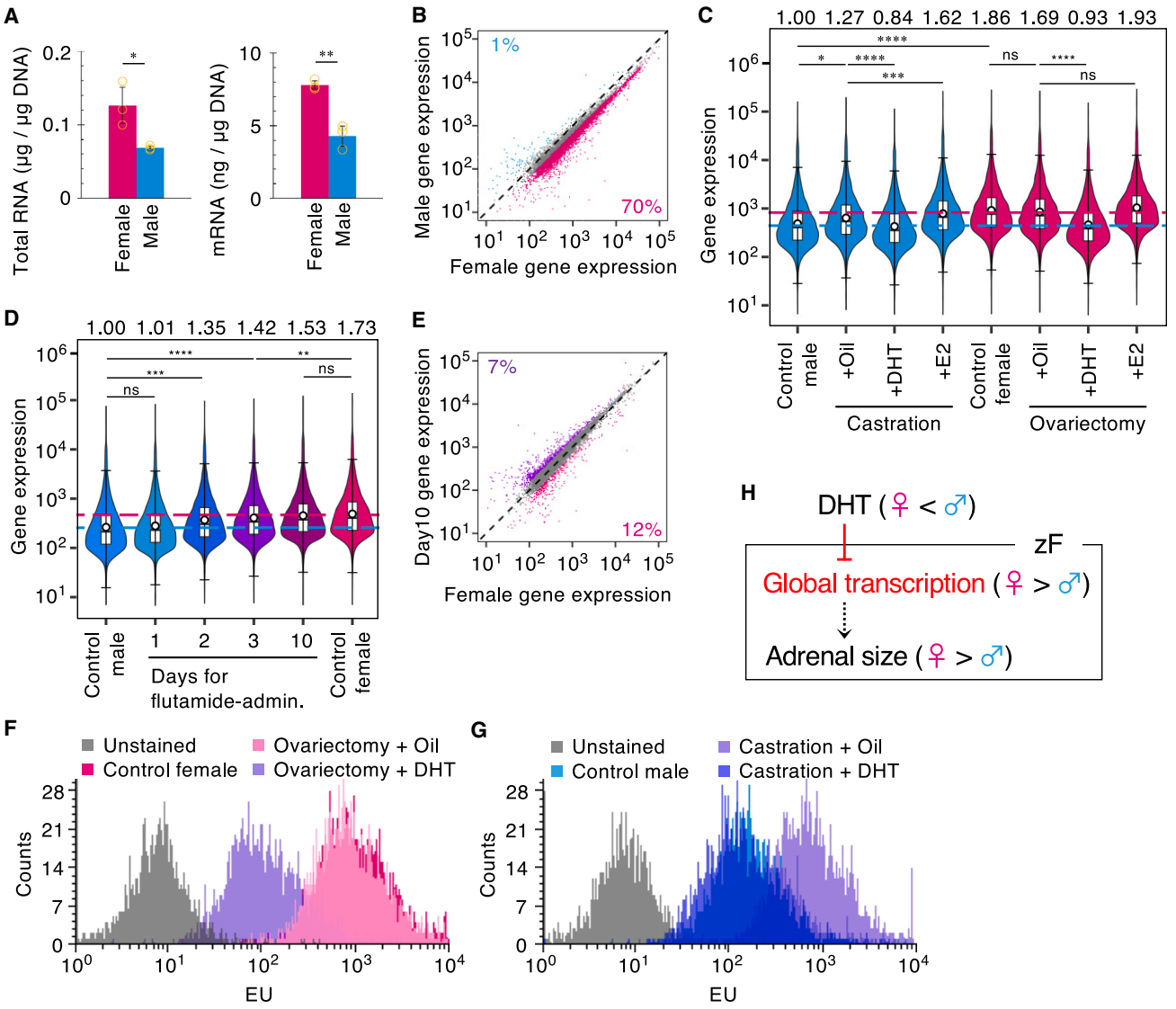

Figure 2. Transcription of zF cells is globally suppressed by DHT

(A) The amounts of total RNA (left) and mRNA (right) zF cells normalized by the amounts of genomic DNAs in female and male zF cells.

(B) A comparison of gene expression (normalized read counts) between females (horizontal axis) and males (vertical axis). Magenta and cyan dots indicate genes highly expressed in females (>1.5-fold higher than males, $p < 0.001$) and genes highly expressed in males (>1.5-fold higher than females, $p < 0.001$), respectively. Proportions of genes represented by magenta and cyan dots are shown.

(C) Violin plots of gene expression levels of the eight experimental groups. Cyan and magenta broken lines indicate the mean gene expression of males and females, respectively. For boxplots, box boundaries represent the 25th and 75th percentiles, whiskers represent the 5th and 95th percentiles, and circles represent the mean. Relative values of whole gene expression are indicated at the top. The value of the male control is set to 1.0.

(D) Violin plots of gene expression levels of flutamide-treated male mice for the days indicated (n = 3).

(E) A comparison of gene expressions between females (horizontal axis) and males treated with flutamide for 10 days (day 10, vertical axis). Magenta and purple dots indicate genes highly expressed in females (>1.5-fold higher than day 10, $p < 0.001$) and genes highly expressed in day 10 (>1.5-fold higher than females, $p < 0.001$), respectively.

(F and G) Representative histograms of nascent transcripts labeled by 5-ethynyl uridine (EU) in zF cells of females (F) and males (G).

(H) DHT downregulates global gene expression in adrenocortical zF cells (red line). Female, ♀; male, ♂.

Data are represented as means ± SDs (A), scatterplot (mean of 3 biological replicates, B and E), or combination of violin and boxplots (C and D). n = 3 biological replicates. *$p < 0.05$, **$p < 0.01$, ***$p < 0.001$, ****$p < 0.0001$, and ns (not significant) by Student's t test (A) or Bonferroni multiple comparison tests (C and D). See also Figures S2 and Table S2.

A

Term	*P*-value
Metabolic pathways	5.84E-24
Huntington disease	3.78E-12
Parkinson disease	4.16E-12
Oxidative phosphorylation	9.70E-12
Amyotrophic lateral sclerosis	4.95E-11
Diabetic cardiomyopathy	3.88E-10
Carbon metabolism	6.24E-10
Thermogenesis	7.84E-10
Prion disease	1.41E-09
Pathways of neurodegeneration - multiple diseases	5.21E-09
Chemical carcinogenesis - reactive oxygen species	8.70E-09
Alzheimer disease	1.07E-08
Valine, leucine and isoleucine degradation	2.16E-07
Protein processing in endoplasmic reticulum	4.91E-07
Citrate cycle (TCA cycle)	9.90E-07
Proteasome	3.13E-06
Non-alcoholic fatty liver disease	4.00E-06
Spliceosome	4.33E-06
Autophagy - animal	1.72E-05
Peroxisome	4.29E-05
Fatty acid degradation	6.44E-05
Glycolysis / Gluconeogenesis	6.52E-05
Biosynthesis of amino acids	9.16E-05
Pyruvate metabolism	1.01E-04
Biosynthesis of cofactors	1.81E-04
Fatty acid metabolism	2.21E-04
RNA degradation	2.44E-04
Spinocerebellar ataxia	4.72E-04
Cortisol synthesis and secretion	5.71E-04
RNA polymerase	7.80E-04
Ribosome biogenesis in eukaryotes	8.40E-04

C

Term	*P*-Value
MAPK signaling pathway	1.78E-06
C-type lectin receptor signaling pathway	8.96E-05
Pathways in cancer	2.95E-04
Proteoglycans in cancer	5.15E-04
Apoptosis	6.22E-04
p53 signaling pathway	6.30E-04

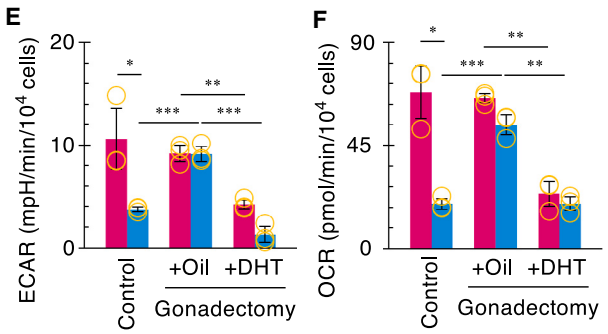

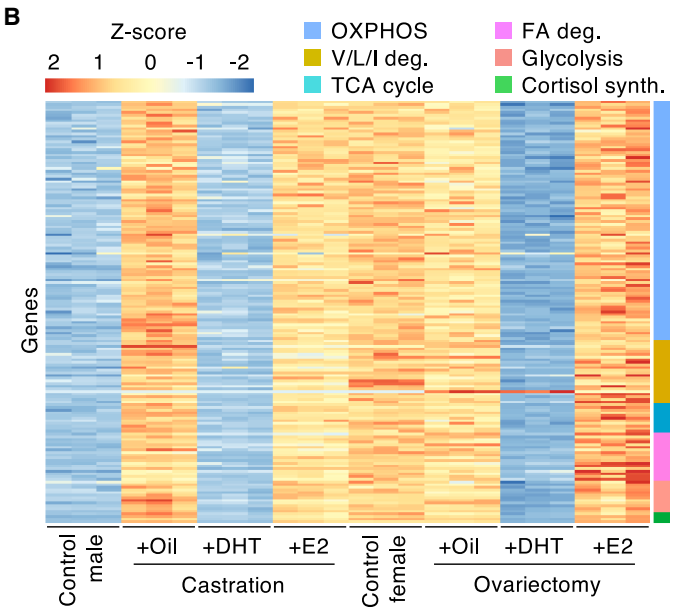

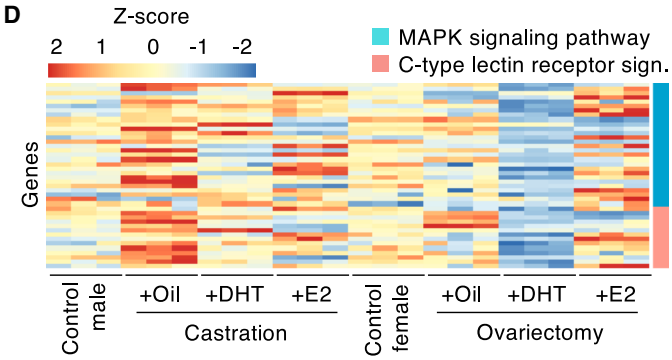

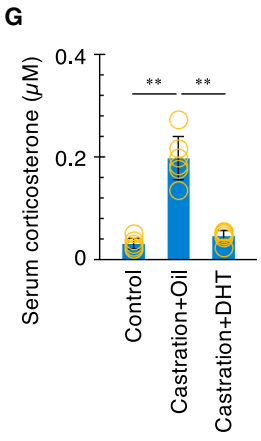

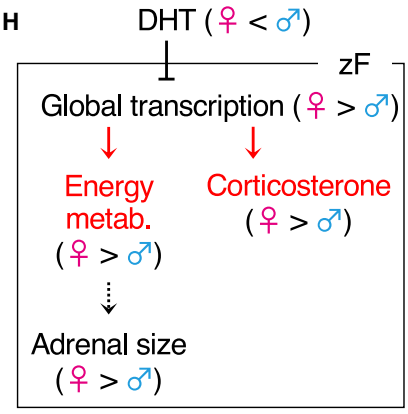

Figure 3. Energy metabolism is more active in female than in male zF cells

(A) The result of KEGG pathway analysis using 2,451 female-biased genes. Terms related to energy metabolism and cortisol synthesis are highlighted in gray.

(B) Expression levels of genes in "oxidative phosphorylation (OXPHOS)," "valine, leucine, and isoleucine degradation (V/L/I deg.)," "TCA cycle," "fatty acid degradation (FA deg.)," "glycolysis and gluconeogenesis (Glycolysis)," and "cortisol synthesis and secretion (Cortisol synth.)" are shown as a heatmap (n = 3 biological replicates).

(legend continued on next page)

3F, glycolytic (extracellular acidification rate [ECAR]) and OXPHOS (oxygen consumption rate [OCR]) activities were approximately 2.83- and 3.51-fold higher, respectively, in females than males. Both activities increased after castration and decreased with DHT treatment in males. Likewise, the activities in ovariectomized females decreased with DHT treatment even though they were not altered merely by ovariectomy (Figures 3E and 3F). These results suggested that the sex differences in glycolytic and OXPHOS activities were attributable to the downregulation of the metabolic genes by androgen.

Moreover, we examined serum corticosterone concentration. Expectedly, serum corticosterone was higher in the females than in males, as described previously[6,10] (Figure S3). As shown in Figure 3G, its concentration significantly increased in castrated males and decreased to control levels after DHT treatment, suggesting that the sex difference in serum corticosterone concentration was attributable to the downregulation of the corticosterone synthetic genes by androgen. These results are summarized in Figure 3H: DHT produced by the testis globally suppresses gene transcription in the male zF cells and thereby downregulates zF cell activities such as energy metabolism and corticosterone synthesis. Based on these results, we could reason that the female-biased size and weight of the adrenal gland is due to the female-activated metabolism promoted by lower androgen concentrations in females.

Nr5a1 gene expression is suppressed by DHT

It has been previously reported that the expression of *Nr5a1* is reduced in the adrenal gland of heterozygous *Nr5a1*-knockout (KO) mice (*Nr5a1*$^{+/-}$) and that the size of the adrenal gland of the heterozygote dwarfed that of the wild type.[39] This observation strongly suggested that the amount of expressed *Nr5a1* affects the size of the adrenal gland. Therefore, we compared *Nr5a1* gene expression between female and male zF cells by CNN RT-qPCR studies and our CNN RNA-seq datasets. Both results demonstrated that the expression of *Nr5a1* was approximately 50% lower in males than in females (Figure 4A). Consistent with this, a western blot study using the same number of zF cells showed that the amount of NR5A1 protein was reduced in males compared to females, although that of histone H3 was unlikely to be different between the two sexes (Figures 4B and S4A).

Next, we examined whether the expression of *Nr5a1* is affected in the zF cells of the eight experimental groups. Castration increased the expression of *Nr5a1*, while ovariectomy decreased it (Figure 4C). DHT treatments after gonadectomy resulted in a significant decrease in expression, back to the level of the male control in both sexes. Interestingly, E2 treatment of the ovariectomized female increased the expression of *Nr5a1* but the same treatment of the castrated male did not increase it. As for the protein level, the amount of NR5A1 in the male control was increased by castration, while that in females was unlikely affected by ovariectomy (Figures 4D and S4B). DHT treatment following gonadectomy decreased NR5A1 in both sexes. By contrast, it was unclear whether E2 treatment had any effect on the protein level.

In addition to western blotting, we attempted to visualize the expression of *Nr5a1* using *Ad4BP-BAC-EGFP* transgenic mice, in which the expression is recapitulated by the expression of EGFP.[40] As shown in Figure 4E, the intensity of EGFP fluorescence was stronger in the female than in the male adrenal gland. The fluorescence in males was enhanced by castration, while it was unlikely that the fluorescence in females was affected by ovariectomy. The fluorescence was largely suppressed by DHT treatment, although it was unlikely to be affected by E2 treatment after gonadectomy.

To further investigate the effect of androgen, flutamide was administered to mice for up to 10 days (Figure S2H), and the expression of *Nr5a1* mRNA was examined by CNN RNA-seq. Expectedly, *Nr5a1* mRNA was increased gradually as the term for flutamide administration (Figure 4F). As shown in Figure 4G, these results strongly suggest that DHT, at least in part, causes the generation of the sexually dimorphic expression of *Nr5a1*.

Gene expression in zF cells is regulated globally by Nr5a1

Considering that NR5A1 is a key transcription factor responsible for the development of the adrenal cortex,[19,21,22] we next examined the possibility that the global decrease in gene expression in the male zF cells could be attributed to the male-suppressed expression of *Nr5a1*. This possibility was examined by the two studies described as follows. First, we examined the effect of the *Nr5a1* gene dosage on the gene expression in *Nr5a1*$^{+/-}$ zF. CNN RNA-seq and CNN RT-qPCR revealed that the expression of *Nr5a1* in the *Nr5a1*$^{+/-}$ cells was less than 20% of the wild type in both sexes (Figure 5A). Similarly, the amount of NR5A1 protein was largely decreased in the heterozygous cells (Figures 5B and S5A). Concerning the expression of whole genes, CNN RNA-seq using the same number of wild-type and *Nr5a1*$^{+/-}$ zF cells clearly indicated that the gene expression decreased globally and to a large degree in the heterozygous cells in both sexes (Figure 5C; Tables S1 and S2). The average expression levels of whole genes in the heterozygous female and male were 6.3% and 19.0% of the wild type, respectively. Moreover, the stronger transcriptional suppression in females resulted in the disappearance of female-biased expression of the global genes;

(C) The result of KEGG pathway analysis using 812 female-unbiased genes.
(D) Expression levels of genes in "MAPK signaling pathway" and "C-type lectin receptor signaling pathway" are shown.
(E and F) ECAR and OCR of zF cells in 6 experimental groups of mice (control, gonadectomy+oil, and gonadectomy+DHT females and males). Magenta and cyan bars indicate female and male zF cells, respectively.
(G) Serum corticosterone (n = 6) in 3 experimental groups of mice (control male, castration+oil, and castration+DHT).
(H) DHT downregulates global gene expression in adrenocortical zF cells, possibly thereby suppressing energy metabolism and corticosterone synthesis (red arrows). The lower activity of energy metabolism may induce the smaller size of adrenal glands of males.
Data are represented as means ± SDs (E–G). n = 3 biological replicates. *p < 0.05, **p < 0.01, and ***p < 0.001 by Bonferroni multiple comparison tests (E–G).
See also Figure S3 and Table S2.

CellPress
OPEN ACCESS

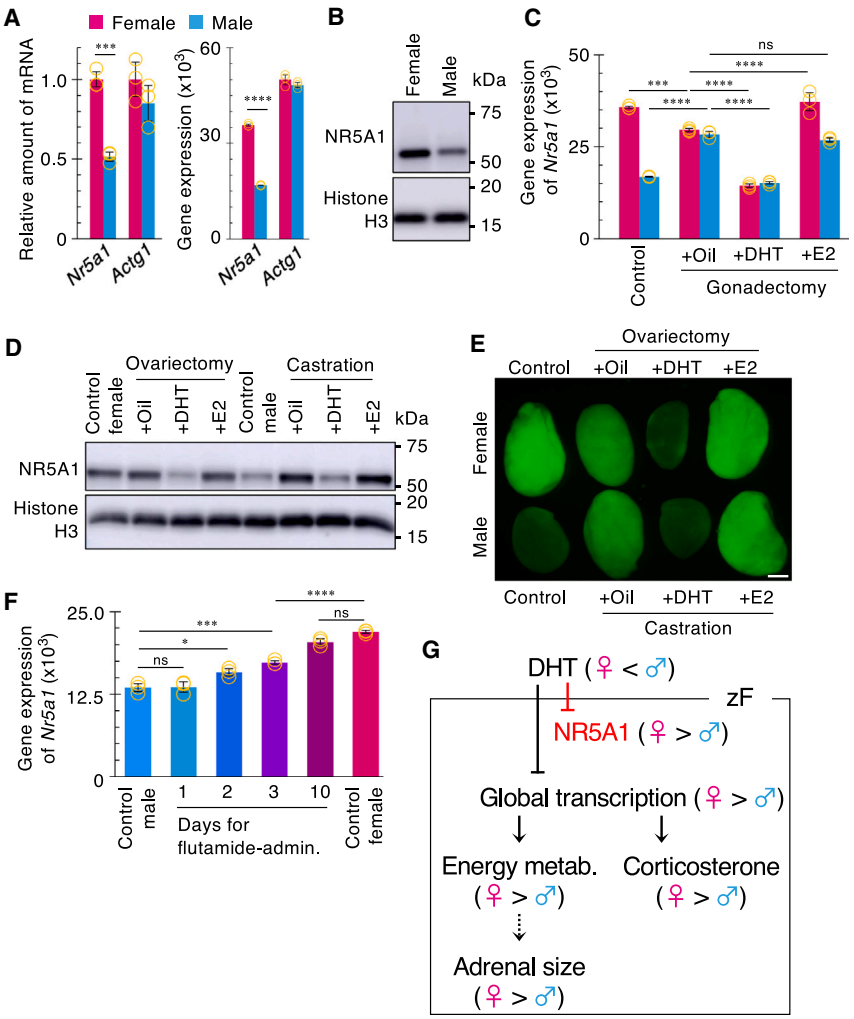

Figure 4. Nr5a1 gene expression is suppressed by DHT

(A) Expression of *Nr5a1* in female and male zF cells examined by CNN RT-qPCR (left) and CNN RNA-seq (right) (normalized read counts). γ-Actin (*Actg1*) was used as a control.

(B) Immunoblotting for NR5A1 using male and female zF cells. α-pan-Histone H3 was used as a control.

(C) Expression of *Nr5a1* calculated using the CNN RNA-seq data of the eight experimental groups (n = 3).

(D) Immunoblotting for NR5A1 using zF cells of the eight groups.

(E) EGFP fluorescence images of adrenal glands of the eight groups of *Ad4BP-BAC-EGFP* transgenic mice. Scale bar represents 500 μm.

(F) Expression levels of *Nr5a1* in zF cells of flutamide-treated male mice determined by CNN RNA-seq.

(G) Similarly to the global gene, the expression of *Nr5a1* was female biased and suppressed by DHT (red line).

Data are represented as means ± SDs (A, C, and F). n = 3 biological replicates. *p < 0.05, ***p < 0.001, ****p < 0.0001, and ns (not significant) by Bonferroni multiple comparison tests (A, C, and F). Uncropped immunoblot images are available in Mendeley Data (see key resource table).

See also Figure S4 and Table S2.

the levels of gene expression in the heterozygous zF cells were comparable between the two sexes (Figure 5D). As NR5A1 plays a crucial role in the production of sex steroids in gonads, sex steroid concentrations in sera were investigated in *Nr5a1*$^{+/-}$ mice. Consequently, it was found that the concentrations of neither testosterone nor E2 were altered in *Nr5a1*$^{+/-}$ mice (Figures S6A and S6B), excluding a possibility that altered circulating levels of the sex steroids in *Nr5a1*$^{+/-}$ mice could cause the disappearance of the sexually dimorphic global gene expression. This simultaneous decrease of *Nr5a1* and whole-gene expression suggests that NR5A1 is involved in the regulation of global gene expression. Nascent RNA synthesis in *Nr5a1*$^{+/-}$ mice decreased in comparison to control mice in both sexes (Figure 5E).

Second, we examined which genes are the potential targets of NR5A1. zF cells were subjected to CUT&RUN-seq analysis. Consequently, 24,051 and 15,033 peaks were identified with female and male zF cells, respectively (Figure 5F; Table S5). Of these, 13,637 peaks were detected to be in common in both sexes, while 10,414 and 1,396 peaks were classified as female-specific and male-specific peaks, respectively. The consensus binding sequence for NR5A1[17] was localized in 99.0% and 98.9% of the NR5A1 peaks detected in females and males, respectively (Figures 5G and S5B). Considering that the amount of NR5A1 protein is greater in females than in males, its accumulation levels at the peaks described previously were expected to be more abundant in females than in males. Indeed, most peaks were larger in females than in males (Figure 5H).

The CUT&RUN-seq data were further analyzed to identify potential target genes of NR5A1. With respect to the location of the peaks, 80.9% and 81.5% of the peaks were localized within gene-proximal regions including upstream (<10 kb from the transcription initiation site), intragenic, and downstream (<10 kb from the transcription termination site) in females and males, respectively. Since 53.2% is the gene-proximal region in the mouse genome, the NR5A1 peaks were likely to be enriched in the proximal regions of potential target genes (Figure 5I). The following studies were performed based on the assumption that the genes localized within 10 kb of the peaks are the direct targets of NR5A1. According to this criterion, 9,287 and 6,858 genes were tentatively identified as potential target genes in the female and male zF cells, respectively (Figures 5J and 5K; Table S6).

As described previously, our CNN RNA-seq studies detected the expression of 7,200 and 7,007 genes in female and male zF cells, respectively. Among these genes, we examined which genes are potential targets for NR5A1 and found that 4,541 genes (63.1% of the expressed genes) in females and 3,475

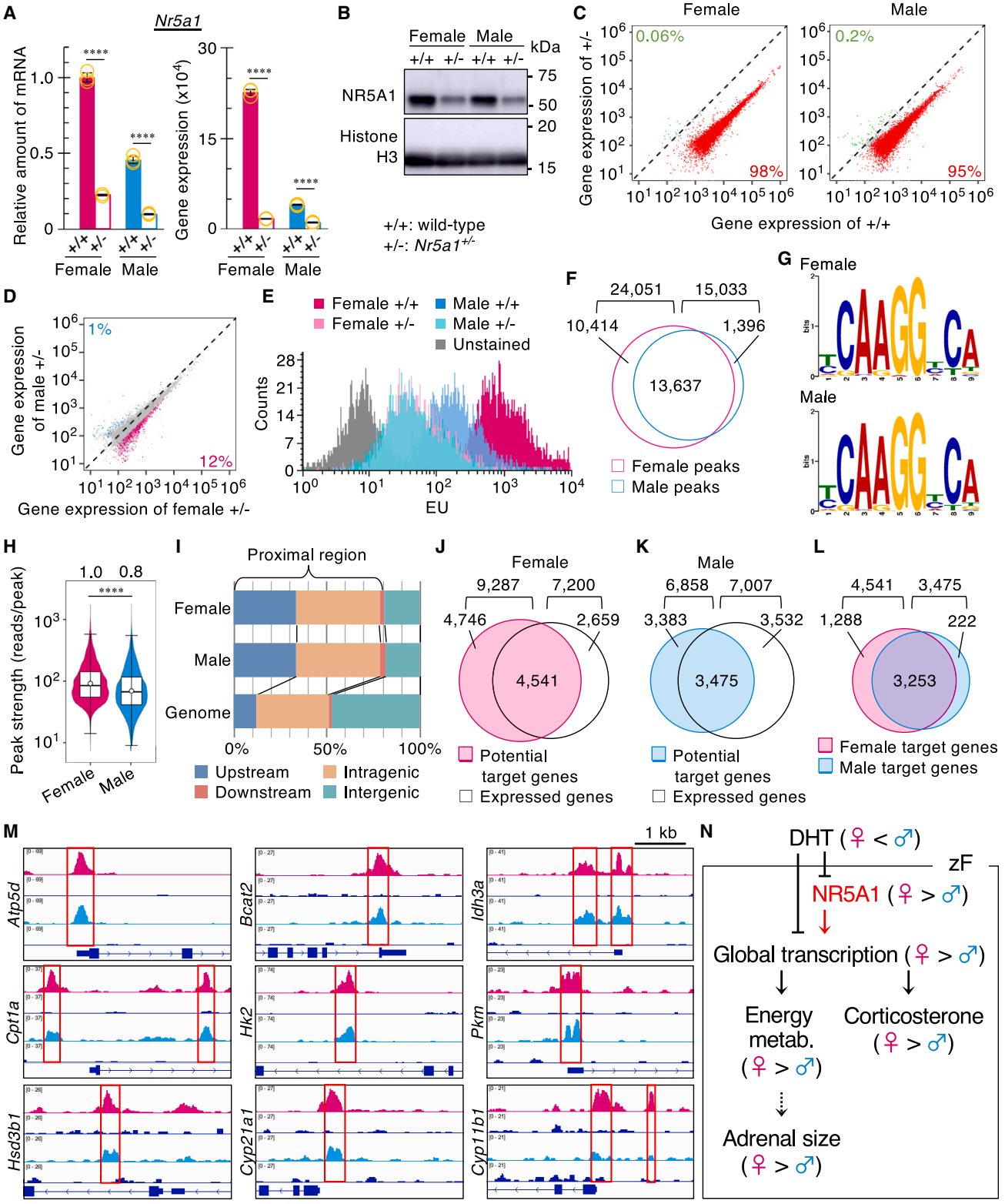

Figure 5. Global gene expression in zF cells is regulated by Nr5a1

(A) Expression of *Nr5a1* in zF cells of wild-type (+/+) and *Nr5a1*$^{+/-}$ (+/−) mice determined by CNN RT-qPCR (left) and CNN RNA-seq (right, normalized read counts).

(legend continued on next page)

(49.6% of the expressed genes) in males are potential targets (Figures 5J and 5K). These target genes were further compared between the two sexes, and 3,253 genes were found to be the targets common to both sexes (Figure 5L). These results suggest that a considerable number of genes are directly regulated by NR5A1 in the adrenal zF cells of both sexes.

Next, we examined whether NR5A1 accumulates at the genes implicated in energy metabolisms and cortisol synthesis. As shown in Figure 5M, the accumulation was observed at *Atp5d* (OXPHOS), *Bcat2* (valine, leucine, and isoleucine degradation), *Idh3a* (TCA cycle), *Cpt1a* (fatty acid degradation), *Hk2* and *Pkm* (glycolysis), and *Hsd3b1*, *Cyp21a1*, and *Cyp11b1* (cortisol synthesis) gene loci. In addition to these genes, the peaks were found in all other genes implicated in these metabolic processes (Figures S5C–S5I). Taken together, the data obtained from the transcriptome studies using heterozygous *Nr5a1*-KO mice and from the CUT&RUN analysis suggested that NR5A1 could mediate the global gene suppression by DHT in zF cells (Figure 5N).

Metabolic activities are decreased in zF cells of heterozygous Nr5a1-KO mice

We compared the expression of OXPHOS, TCA cycle, glycolytic, and corticosterone synthetic genes using the transcriptome datasets obtained from wild-type and $Nr5a1^{+/-}$ zF cells. As mentioned previously, these gene expressions in the wild type were higher in females than in males (Figure 6A). As expected, the expression of these genes was largely decreased in $Nr5a1^{+/-}$ zF cells in both sexes. Interestingly, however, the $Nr5a1^{+/-}$ zF cells failed to show any sex difference in the expression of these metabolic genes.

Subsequently, we determined the ECAR and OCR of wild-type and $Nr5a1^{+/-}$ zF cells. The ECAR of the $Nr5a1^{+/-}$ female was decreased to 39.5% of the wild-type female. Likewise, the activity of the $Nr5a1^{+/-}$ male was decreased to the level of the $Nr5a1^{+/-}$ female (Figure 6B). The OCR of the $Nr5a1^{+/-}$ female zF cells was decreased to 67.4% of the wild type, whereas the activity was not decreased in the $Nr5a1^{+/-}$ male compared to the wild type (Figure 6C). Consistent with the altered energy metabolism, cellular ATP concentration in the $Nr5a1^{+/-}$ zF cells was decreased to 56.2% in wild-type females, while it was decreased to 65.6% in males (Figure 6D). Furthermore, the concentration of serum corticosterone in $Nr5a1^{+/-}$ zF cells decreased to 25.6% of that in wild-type females, while it decreased to 9.2% in males (Figure 6E).

NADPH has been known to be required for multiple anabolic pathways including steroidogenesis.[41] We previously reported that NR5A1 regulates cellular NADPH production in Y-1 cells through regulating transcription of key genes.[29] As shown in Figure 6F, the expressions of the key genes *G6pdx* and *Pgd* in the pentose phosphate shunt, *Mthfd1* in one-carbon metabolism, *Me2*, *Idh1*, and *Idh2* were all female biased in zF cells. Moreover, accumulation of NR5A1 was observed all at the gene loci (Figures S5E and S5I), suggesting that these genes are all potential targets of NR5A1. In fact, the heterozygous KO of the *Nr5a1* gene led to a marked decrease in the NADPH synthetic gene expression. However, similarly to the energy metabolic genes, the sexually different expression of the genes became less obvious or disappeared in the $Nr5a1^{+/-}$ zF cells. Consistently, the amount of NADPH in zF cells was higher in females than in males, and the female-biased amount of NADPH became lower with the heterozygous KO of *Nr5a1* gene (Figure 6G).

Size and weight of skeletal muscles may be regulated by the expression of Nr5a1 in zF cells

Recent studies showed the direct implication of androgen receptor (AR) in the increase of grip strength rather than the size of skeletal muscles.[42–45] Therefore, it has been speculated that the size of the skeletal muscles is indirectly regulated by androgens.[46] Skeletal-muscle-specific KO of the glucocorticoid receptor (GR) induces muscle hypertrophy,[47] while administration of dexamethasone, a chemical analog of cortisol, induces hypotrophy of skeletal muscles.[5] It has also been reported that serum corticosterone is largely decreased in $Nr5a1^{+/-}$ mice under

(B) Immunoblotting for NR5A1. α-pan-Histone H3 was used as a control.
(C) A comparison of gene expression between $Nr5a1^{+/-}$ (+/−, horizontal) and wild-type (+/+, vertical axis) zF cells of females (left) and males (right). Orange and green dots indicate genes highly expressed in wild type (>1.5-fold higher than $Nr5a1^{+/-}$, $p < 0.001$) and genes highly expressed in $Nr5a1^{+/-}$ (>1.5-fold higher than wild type, $p < 0.001$), respectively. Proportions of genes represented by orange and green dots are shown.
(D) A comparison of gene expression between $Nr5a1^{+/-}$ female (horizontal axis) and $Nr5a1^{+/-}$ male (vertical axis) zF cells. Magenta and cyan dots indicate genes highly expressed in females (>1.5-fold higher than males, $p < 0.001$) and genes highly expressed in males (>1.5-fold higher than females, $p < 0.001$), respectively.
(E) Representative histograms of nascent transcripts labeled by 5-EU in zF cells of 5 groups of mice (unstained wild-type female, wild-type female, $Nr5a1^{+/-}$ female, wild-type male, and $Nr5a1^{+/-}$ male).
(F) A Venn diagram showing overlap of NR5A1 CUT&RUN-seq peaks between females and males.
(G) Nucleotide sequences extracted from the NR5A1 peaks for females and males.
(H) Comparison of strength of NR5A1 peaks evaluated by the number of mapped reads between females and males (n = 2 biological replicates).
(I) Genomic location of NR5A1 peaks relative to their nearest genes.
(J and K) A Venn diagram showing an overlap between the expressed genes and potential target genes of NR5A1 in female (J) and male (K) zF cells.
(L) An overlap of the target genes between females and males.
(M) Magenta and cyan histogram indicate accumulation of NR5A1 CUT&RUN products obtained from female and male zF cells, while blue indicates that of control immunoglobulin G (IgG). Exon and intron structures of the genes indicted are shown at the bottom.
(N) Transcriptome and CUT&RUN-seq datasets suggest the presence of a large number of potential target genes for NR5A1 in zF cells. Global gene suppression by DHT might be mediated directly or indirectly by NR5A1 (red arrow).
Data are represented as means ± SDs (A), scatterplot (mean of 3 biological replicates, C and D), or combination of violin and boxplot (H). n = 3 biological replicates. ****$p < 0.0001$ by Bonferroni multiple comparison tests (A) or Mann-Whitney's non-parametric test (H). Uncropped immunoblot images are available in Mendeley Data (see key resource table).
See also Figure S5 and Tables S5, S6, and S7.

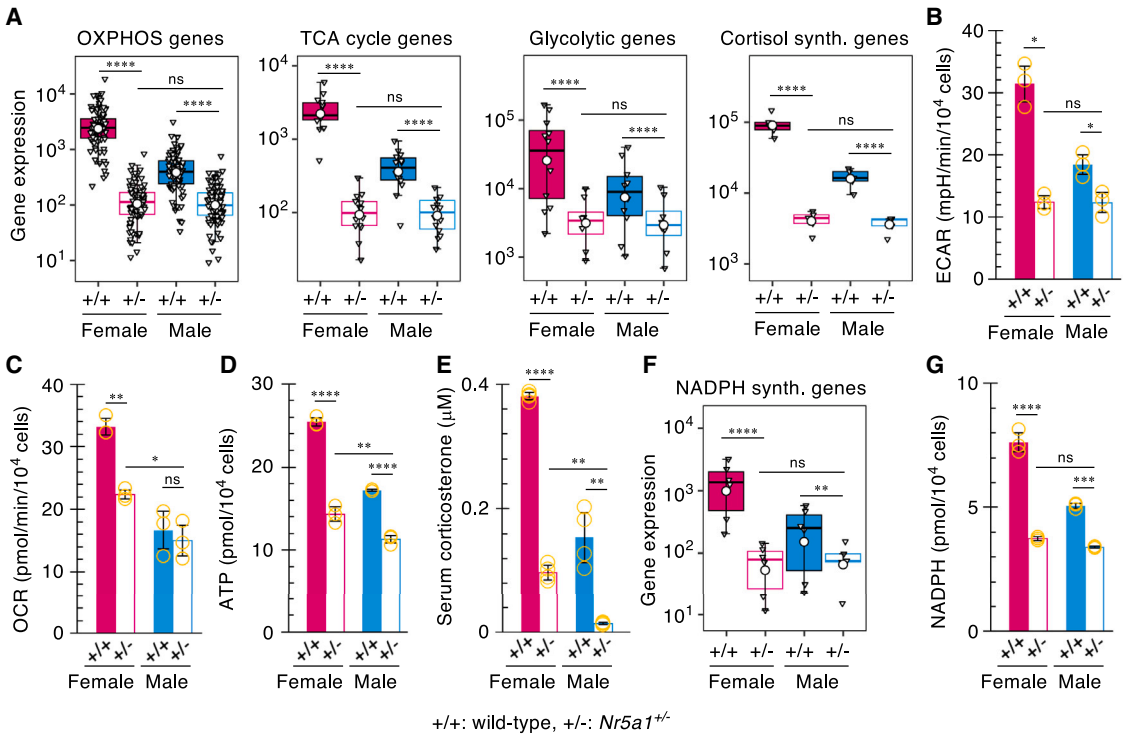

Figure 6. Metabolic activities are decreased in zF cells of heterozygous Nr5a1-knockout mice

(A) Expression levels (normalized read counts) of OXPHOS, TCA cycle, glycolytic, and corticosterone synthetic genes calculated using CNN RNA-seq datasets obtained from wild-type (+/+) and *Nr5a1*$^{+/-}$ (+/−) zF cells of the two sexes.

(B–D) ECAR (B), OCR (C), and intracellular ATP (D) of zF cells.

(E) Serum corticosterone concentration of wild type (+/+) and *Nr5a1*$^{+/-}$ (+/−) in both sexes.

(F) Expression levels of NADPH synthetic genes (n = 3).

(G) Intracellular NADPH levels of the zF cells.

Data are represented as a boxplot (A and F) or means ± SDs (B–E and G). n = 3–4 biological replicates. *p < 0.05, **p < 0.01, ***p < 0.001, ****p < 0.0001, and ns (not significant) by Wilcoxon signed rank tests (A and F) or Bonferroni multiple comparison tests (B–E and G).

See also Figure S6.

stress conditions.[39] Considering these results, we assumed that the size and weight of the skeletal muscles of *Nr5a1*$^{+/-}$ mice are increased by the decreased corticosterone.

Under this assumption, we investigated the skeletal muscles of *Nr5a1*$^{+/-}$ mice. As expected, the muscles of the forelimb and hindlimb were obviously larger in *Nr5a1*$^{+/-}$ than in wild-type mice in both sexes (Figure 7A). Consistent with this, the weights of the gastrocnemius, quadriceps, and triceps of *Nr5a1*$^{+/-}$ mice were all higher than those of the wild type in both sexes (Figure 7B). The skeletal muscles consist of multiple types of fibers, in which type IIB fibers dominate in the fast-twitch muscles in rodents. Cross-sections of wild-type and *Nr5a1*$^{+/-}$ gastrocnemius, quadriceps, and triceps were subjected to immunostaining for the marker of the type IIB fiber (myosin heavy chain 4) (Figures 7C, S7A, and S7B). Then, the cross-sectional areas (CSAs) of the type IIB fibers of the muscles were determined (Figures 7D, 7E, and S7C–S7F). Consistent with previous reports,[48] the CSAs of the type IIB fibers of these muscles were larger in males than in females in the wild type. As expected, the CSAs of the gastrocnemius type IIB fibers were found to be significantly larger in the *Nr5a1*$^{+/-}$ than in the wild type in both sexes. Likewise, the CSAs of the quadriceps and triceps muscles displayed similar changes in *Nr5a1*$^{+/-}$ mice (Figures S7C–S7F). Comparison of the four muscles (wild-type male and female and *Nr5a1*$^{+/-}$ male and female) indicated that disruption of a single *Nr5a1* allele made the CSA larger in both sexes. Interestingly, the CSA of the *Nr5a1*$^{+/-}$ females became larger approximately to the level of wild-type males. Taken together, our results strongly suggested that the quantity of the *Nr5a1* gene is responsible for the regulation of the muscle size and weight. Finally, our present study could provide a novel mechanism for establishing and maintaining the sexually dimorphic structure and function of the skeletal muscles, in which androgen synthesized in the testis indirectly induces male-biased enlargement of the skeletal muscles through suppression of glucocorticoid synthesis (Figure 7F).

DISCUSSION

This study aims to demonstrate the mechanism of adrenocortical sex differentiation and the physiological significance of the sexually different adrenal cortex. Consequently, we obtained two interesting results: one is the mechanism for sex

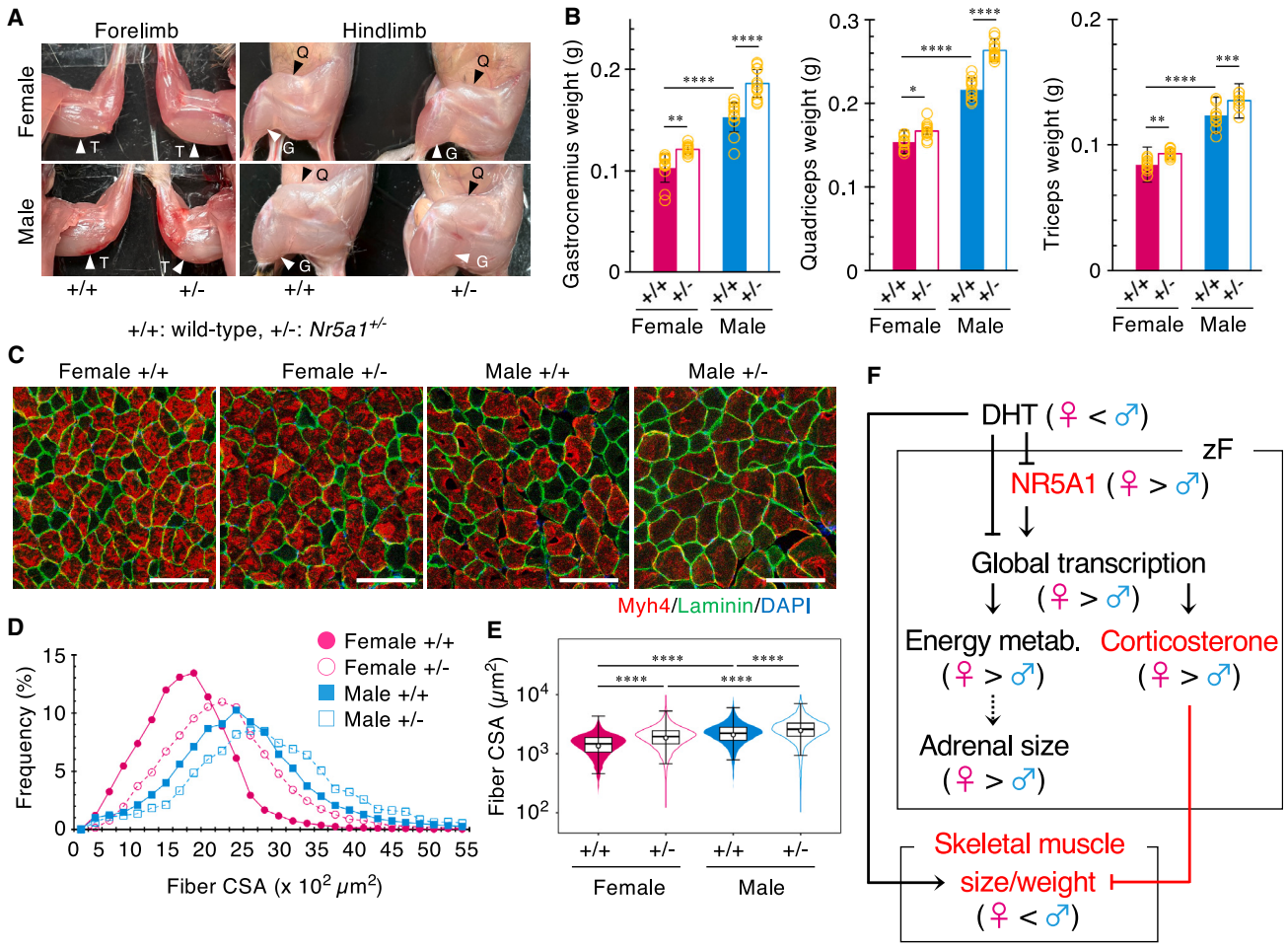

Figure 7. Size and weight of skeletal muscles may be regulated by the expression of Nr5a1 in zF cells

(A) Representative images of skeletal muscles of the forelimbs (left) and hindlimbs (right) of wild-type (+/+) and *Nr5a1*$^{+/-}$ (+/−) mice (12 weeks old). G, Q, and T indicate the gastrocnemius, quadriceps, and triceps muscles, respectively.

(B) Weights of gastrocnemius, quadriceps, and triceps muscles of wild-type (+/+) and *Nr5a1*$^{+/-}$ (+/−) mice of the two sexes (n = 12).

(C) Representative images of the immunostaining of transverse cryosections of the gastrocnemius from wild-type (+/+) and *Nr5a1*$^{+/-}$ (+/−) mice of the two sexes. Type IIb myosin heavy chain 4 (red), laminin (green), and nuclei (blue) were stained. Scale bars represent 100 μm.

(D) CSAs of gastrocnemius type IIB fibers of wild-type (+/+) and *Nr5a1*$^{+/-}$ (+/−) mice of the two sexes. The distribution of CSA sizes (horizontal axis) and frequencies (vertical axis) is shown.

(E) The CSAs of the type IIB fibers above are presented with violin plots.

(F) All results obtained by the present study are summarized.

Data are represented as means ± SDs (B), histogram (mean of 3 biological replicates) (D), or combination of violin and boxplot (mean of 3 biological replicates) (E). n = 3 biological replicates. *p < 0.05, **p < 0.01, ***p < 0.001, and ****p < 0.0001 by Bonferroni multiple comparison tests (B and E).

See also Figure S7.

differentiation regulated by the adrenal cortex and the other is the mechanism for sex differentiation by global gene regulation.

A novel mechanism for sex differentiation regulated by the adrenal cortex

To explore how the sexually dimorphic adrenal cortex develops, it was essential to obtain transcriptomes from both sexes. The adrenal cortex consists of three distinct zones, the zG, zF, and zone reticularis (the last zone is not present in rodents). Among these zones, we focused on the zF, which produces glucocorticoid. After zF cells were highly purified from the male and female adrenal cortices, mRNAs were prepared. Surprisingly, the amount of the mRNA was 1.82-fold greater in females even though the same number of cells were utilized. Similarly to the size of the adrenal gland decreased by androgen,[49] the amounts of mRNA were decreased by the same sex steroid.

Although androgen has generally been thought to activate gene expression via binding to the receptor,[50] the suppressive action of androgen has been often studied. There are two possible mechanisms for this suppression. One is the direct suppression of gene expression in the adrenal cortex by androgen, and this is supported by the evidence that the adrenal gland of

the adrenocortical-specific AR KO mouse was enlarged.[51] The other is the indirect suppression through other types of cells. To date, studies have demonstrated that androgen suppresses the hypothalamus-pituitary-adrenal axis and then decreases adrenocorticotropic hormone (ACTH).[52,53] Because ACTH activates adrenocortical cell proliferation and corticosterone synthesis,[54] it is reasonable to assume that androgen decreases corticosterone synthesis indirectly through decreasing ACTH synthesis.

Accordingly, we assumed that higher serum corticosterone in females, caused by an enlarged adrenal cortex, could ultimately induce sex differences in other cell types. In fact, skeletal muscle fibers and hepatocytes could be such examples where sexually different features are affected by glucocorticoids. The sexually dimorphic size of the skeletal muscle is affected by the muscle-specific GR KO,[47] and the sexually different expression of inflammatory genes in the liver is affected by liver-specific GR KO.[55] In addition to these studies, we examined the possible implication of glucocorticoids into sex differentiation using *Nr5a1* heterozygous mice, whose serum corticosterone is significantly decreased.[39] As expected, the weight and CSA of type IIB fibers of the skeletal muscles were found to be larger in the heterozygous mice. Because the GR is expressed in many cell types, glucocorticoid is thought to be involved in the establishment of sex differences in other parts of the body, in addition to muscle fibers and hepatocytes. Until now, sex differences were thought to be induced directly by sex hormones and their receptors. Going forward, regulation by glucocorticoid and the GR should also be considered when studying and discussing sex differences.

Mechanism for sex differentiation by global gene regulation

To investigate adrenocortical sex differences, two research groups adopted a microarray technique to analyze gene expression.[14–16] These studies successfully identified sexually dimorphic gene expression. One of the studies demonstrated that testosterone stimulates expressions of the genes associated with lipid and cholesterol metabolisms. Unfortunately, however, their results were not completely consistent with our study. The discrepancy could be derived from differences in the materials used in the two studies. Our study used mRNA prepared from highly purified mouse zF cells, whereas their studies used RNA prepared from rat zF and zG[14] or RNA prepared from whole adrenal glands of rats.[15] When comparing the results obtained from a material of highly purified cells versus material containing contaminant cells, more accurate results could be obtained from the former material. Moreover, because the amounts of RNA per zF cell differ between the two sexes, we used RNAs prepared from the same number of male and female zF cells. By contrast, the same amounts of female and male RNA were used in their studies. When comparing two types of cells whose mRNA contents are different, transcriptomes using the same amount of mRNA may not reflect the characteristics of the target cells. Therefore, when handling transcriptome data obtained without any consideration of this issue, close attention would be required.

Comparison of the gene expressions of zF cells between the two sexes revealed that nearly all gene expression is higher in females. Global transcriptional regulation like this was indicated to occur during several physiological events such as cancer progression and cellular differentiation.[32–35,56] As a consequence, basic cellular activities such as translation, metabolisms, and cell proliferation were activated. Therefore, such global transcriptional regulation has attracted attention as a novel mechanism to dramatically change the cellular state. Our present study demonstrates that such regulation is adopted to produce sexual dimorphic features of the adrenal cortex in mice and that androgen plays a pivotal role in global transcriptional repression.

Although genes were globally upregulated in female zF cells, there were genes whose expression was higher than average in females. These genes were found to be closely related to biological activities such as the production of energy and lipids; valine, leucine, and isoleucine metabolisms; and the generation of NADPH and cortisol. Showing a good correlation with this, biological activities such as glycolysis, OXPHOS, and NADPH generation were shown to be female biased. ATP and NADPH were utilized for cholesterol synthesis and the steroidogenesis that follows. Accordingly, the female-biased metabolic activities could provide females with a greater potential to produce corticosterone.[57] Likewise, the consumption of ATP and NADPH for the synthesis of DNA, proteins, and membranes is required for cell proliferation. The female-biased metabolic activities could confer the potentiality of higher proliferative activity to female zF cells.

Accumulation of NR5A1 was observed in greater than half of the expressed genes in zF (63.1% for females and 49.6% for males), and approximately 4,500 and 3,500 genes for females and males, respectively, were estimated as the target genes. Moreover, because the expression of nearly all genes was altered in accordance with the level of *Nr5a1* gene expression, this factor is assumed to be deeply involved in global gene regulation in either a direct or indirect way. Thus far, target genes for many transcription factors have been explored at the whole-genome level, and consequently, many transcription factors have been shown to have thousands of target genes.[58,59] Similarly to NR5A1, these transcription factors may potentially be involved in global gene regulation.

AR has been reported to act as a transcriptional suppressor in addition to an activator.[50] Recently, AR has been shown to suppress global gene transcription in prostate cancer by suppressing Myc gene expression.[60] Likewise, our present study indicates the possibility that AR suppresses global gene transcription in zF cells by suppressing *Nr5a1* gene expression. Considering the similarity between the correlation of AR and Myc and that of AR and NR5A1, the global suppression of gene transcription in zF cells is thought to be mediated by NR5A1. In addition to this possibility, our previous study indicated that AR suppressed the transcriptional activity of NR5A1 through direct interaction in the presence of AR ligands.[61] NR5A1 could mediate AR-dependent global gene suppression possibly through these two processes.

Opposing to DHT, E2 increased adrenal weights and global gene expressions (Figures 1A–1C and 2C). It could be considered that E2 exerted the actions opposing to DHT by increasing Nr5a1 expression. However, it was demonstrated that E2 did not impact Nr5a1 expression, whereas DHT significantly decreased

it (Figure S4B). This suggests that the E2-induced actions above are unlikely mediated through the regulation of *Nr5a1*.

It is well accepted that sex hormones and their receptors induce sex differences by regulating target gene expression. In fact, many target genes have been identified, and some sex differences have been realized by the functions of the target genes. In addition to this authentic pathway, our present study unveiled a novel pathway to establish sexual dimorphism throughout the whole body through sexually dimorphic adrenocortical function.

Limitations of the study

It remains controversial whether circulating cortisol levels exhibit sex differences in humans. Therefore, the model proposed in this study, which demonstrates that sex differences in adrenal glucocorticoid production induce sexually dimorphic skeletal muscle size in mice, should not be immediately applicable to humans.

STAR★METHODS

Detailed methods are provided in the online version of this paper and include the following:

- KEY RESOURCES TABLE
- RESOURCES AVAILABILITY
  - Lead contact
  - Materials availability
  - Data and code availability
- EXPERIMENTAL MODEL AND SUBJECT DETAILS
  - Mice
- METHOD DETAILS
  - Sex steroids treatment
  - Flutamide treatment
  - Preparation of zF cells
  - Quantification of total RNA and mRNA prepared from zF tissue
  - Preparation of total RNA and mRNA from zF cells
  - Nascent transcription assay
  - CNN RNA-seq and data processing
  - Measurement of ECAR and OCR
  - Measurement of serum steroids
  - CNN qRT-PCR
  - Immunoblotting
  - CUT&RUN-seq and data processing
  - Quantification of cellular ATP and NADPH
  - Measurement of muscles fiber CSA (cross sectional area)
- QUANTIFICATION AND STATISTICAL ANALYSIS

SUPPLEMENTAL INFORMATION

Supplemental information can be found online at https://doi.org/10.1016/j.celrep.2024.113715.

ACKNOWLEDGMENTS

This work was supported by the Japan Society for the Promotion of Science (JSPS) KAKENHI grant numbers JP16H05142 (K.-i.M.), JP17H06427 (K.-i.M.), JP20H03436 (K.-i.M.), JP20K08863 (T.B.), JP22H04993 (K-i.M., T.B.), JP23K07991 (T.B.), JP21K08565 (H.-C.L.-O.), JP19KK0199 (T.Y.), JP21H04798 (T.Y.), and JP21K19584 (K.H.); the Strategic Research Program for Brain Sciences (SRPBS) from the Japan Agency for Medical Research and Development (AMED) grant number JP21wm0425008s0201 (T.Y.); and the Takeda Science Foundation (T.B.). We thank Takefumi Kikusui (Center for Human and Animal Symbiosis Science at Azabu University) for help with the blood taking of mice. We thank the Research Support Center, Research Center for Human Disease Modeling, Kyushu University Graduate School of Medical Sciences for the technical assistance. The graphical abstract was created with BioRender.com.

AUTHOR CONTRIBUTIONS

F.T., T.B., and K.-i.M. conceived and designed the experimental approach and performed the experiments. F.T., T.B., and K.-i.M. prepared the manuscript. S.Y. performed the CUT&RUN library preparation. K.I., K.N., and K.H. performed deep sequencing of the CUT&RUN libraries. T. I. and T.H. provided the StAR-EGFP transgenic mouse. H.-C.L.-O., T.Y., and M.H.C. performed mass spectrometry analyses. All the authors discussed and read the manuscript.

DECLARATION OF INTERESTS

The authors declare no competing interests.

Received: April 12, 2023
Revised: December 8, 2023
Accepted: January 11, 2024

REFERENCES

1. Xing, Y., Lerario, A.M., Rainey, W., and Hammer, G.D. (2015). Development of adrenal cortex zonation. Endocrinol. Metab. Clin. North Am. *44*, 243–274.
2. Pihlajoki, M., Dörner, J., Cochran, R.S., Heikinheimo, M., and Wilson, D.B. (2015). Adrenocortical zonation, renewal, and remodeling. Front. Endocrinol. *6*, 27.
3. Vinson, G.P. (2016). Functional Zonation of the Adult Mammalian Adrenal Cortex. Front. Neurosci. *10*, 238.
4. Lyraki, R., and Schedl, A. (2021). Adrenal cortex renewal in health and disease. Nat. Rev. Endocrinol. *17*, 421–434.
5. Munck, A., Guyre, P.M., and Holbrook, N.J. (1984). Physiological functions of glucocorticoids in stress and their relation to pharmacological actions. Endocr. Rev. *5*, 25–44.
6. Kitay, J.I. (1963). PITUITARY-ADRENAL FUNCTION IN THE RAT AFTER GONADECTOMY AND GONADAL HORMONE REPLACEMENT. Endocrinology *73*, 253–260.
7. Malendowicz, L.K., Robba, C., and Nussdorfer, G.G. (1986). Sex differences in adrenocortical structure and function. XXII. Light- and electron-microscopic morphometric studies on the effects of gonadectomy and gonadal hormone replacement on the rat adrenal cortex. Cell Tissue Res. *244*, 141–145.
8. Bielohuby, M., Herbach, N., Wanke, R., Maser-Gluth, C., Beuschlein, F., Wolf, E., and Hoeflich, A. (2007). Growth analysis of the mouse adrenal gland from weaning to adulthood: time- and gender-dependent alterations of cell size and number in the cortical compartment. Am. J. Physiol. Endocrinol. Metab. *293*, E139–E146.
9. Malendowicz, L.K. (1974). Sex differences in adrenocortical structure and function. I. The effects of postpubertal gonadectomy and gonadal hormone replacement on nuclear volume of adrenocortical cells in the rat. Cell Tissue Res. *151*, 525–536.
10. Feillet, C., Guérin, S., Lonchampt, M., Dacquet, C., Gustafsson, J.Å., Delaunay, F., and Teboul, M. (2016). Sexual Dimorphism in Circadian Physiology Is Altered in LXRα Deficient Mice. PLoS One *11*, e0150665.

11. Dumontet, T., Sahut-Barnola, I., Septier, A., Montanier, N., Plotton, I., Roucher-Boulez, F., Ducros, V., Lefrançois-Martinez, A.M., Pointud, J.-C., Zubair, M., et al. (2018). PKA signaling drives reticularis differentiation and sexually dimorphic adrenal cortex renewal. JCI Insight *3*, e98394.

12. Grabek, A., Dolfi, B., Klein, B., Jian-Motamedi, F., Chaboissier, M.-C., and Schedl, A. (2019). The Adult Adrenal Cortex Undergoes Rapid Tissue Renewal in a Sex-Specific Manner. Cell Stem Cell *25*, 290–296.e2.

13. Lyraki, R., and Schedl, A. (2021). The Sexually Dimorphic Adrenal Cortex: Implications for Adrenal Disease. Int. J. Mol. Sci. *22*, 4889.

14. Trejter, M., Hochol, A., Tyczewska, M., Ziolkowska, A., Jopek, K., Szyszka, M., Malendowicz, L.K., and Rucinski, M. (2015). Sex-related gene expression profiles in the adrenal cortex in the mature rat: microarray analysis with emphasis on genes involved in steroidogenesis. Int. J. Mol. Med. *35*, 702–714.

15. Jopek, K., Celichowski, P., Szyszka, M., Tyczewska, M., Milecka, P., Malendowicz, L.K., and Rucinski, M. (2017). Transcriptome Profile of Rat Adrenal Evoked by Gonadectomy and Testosterone or Estradiol Replacement. Front. Endocrinol. *8*, 26.

16. El Wakil, A., Mari, B., Barhanin, J., and Lalli, E. (2013). Genomic analysis of sexual dimorphism of gene expression in the mouse adrenal gland. Horm. Metab. Res. *45*, 870–873.

17. Morohashi, K., Honda, S., Inomata, Y., Handa, H., and Omura, T. (1992). A common trans-acting factor, Ad4-binding protein, to the promoters of steroidogenic P-450s. J. Biol. Chem. *267*, 17913–17919.

18. Lala, D.S., Rice, D.A., and Parker, K.L. (1992). Steroidogenic factor I, a key regulator of steroidogenic enzyme expression, is the mouse homolog of fushi tarazu-factor I. Mol. Endocrinol. *6*, 1249–1258.

19. Morohashi, K.I., and Omura, T. (1996). Ad4BP/SF-1, a transcription factor essential for the transcription of steroidogenic cytochrome P450 genes and for the establishment of the reproductive function. FASEB J *10*, 1569–1577.

20. Parker, K.L., and Schimmer, B.P. (1997). Steroidogenic factor 1: a key determinant of endocrine development and function. Endocr. Rev. *18*, 361–377.

21. Luo, X., Ikeda, Y., and Parker, K.L. (1994). A cell-specific nuclear receptor is essential for adrenal and gonadal development and sexual differentiation. Cell *77*, 481–490.

22. Sadovsky, Y., Crawford, P.A., Woodson, K.G., Polish, J.A., Clements, M.A., Tourtellotte, L.M., Simburger, K., and Milbrandt, J. (1995). Mice deficient in the orphan receptor steroidogenic factor 1 lack adrenal glands and gonads but express P450 side-chain-cleavage enzyme in the placenta and have normal embryonic serum levels of corticosteroids. Proc. Natl. Acad. Sci. USA *92*, 10939–10943.

23. Ferraz-de-Souza, B., Lin, L., Shah, S., Jina, N., Hubank, M., Dattani, M.T., and Achermann, J.C. (2011). ChIP-on-chip analysis reveals angiopoietin 2 (Ang2, ANGPT2) as a novel target of steroidogenic factor-1 (SF-1, NR5A1) in the human adrenal gland. FASEB J *25*, 1166–1175.

24. Ju, Y., Mizutani, T., Imamichi, Y., Yazawa, T., Matsumura, T., Kawabe, S., Kanno, M., Umezawa, A., Kangawa, K., and Miyamoto, K. (2012). Nuclear receptor 5A (NR5A) family regulates 5-aminolevulinic acid synthase 1 (ALAS1) gene expression in steroidogenic cells. Endocrinology *153*, 5522–5534.

25. Doghman, M., Figueiredo, B.C., Volante, M., Papotti, M., and Lalli, E. (2013). Integrative analysis of SF-1 transcription factor dosage impact on genome-wide binding and gene expression regulation. Nucleic Acids Res. *41*, 8896–8907.

26. Yamauchi, K., Ikeda, T., Hosokawa, M., Nakatsuji, N., Kawase, E., Chuma, S., Hasegawa, K., and Suemori, H. (2020). Overexpression of Nuclear Receptor 5A1 Induces and Maintains an Intermediate State of Conversion between Primed and Naive Pluripotency. Stem Cell Rep. *14*, 506–519.

27. Baba, T., Otake, H., Sato, T., Miyabayashi, K., Shishido, Y., Wang, C.-Y., Shima, Y., Kimura, H., Yagi, M., Ishihara, Y., et al. (2014). Glycolytic genes are targets of the nuclear receptor Ad4BP/SF-1. Nat. Commun. *5*, 3634.

28. Ruggiero, C., Doghman-Bouguerra, M., Sbiera, S., Sbiera, I., Parsons, M., Ragazzon, B., Morin, A., Robidel, E., Favier, J., Bertherat, J., et al. (2017). Dosage-dependent regulation of *VAV2* expression by steroidogenic factor-1 drives adrenocortical carcinoma cell invasion. Sci. Signal. *10*, eaal2464.

29. Li, B., Baba, T., Miyabayashi, K., Sato, T., Shima, Y., Ichinose, T., Miura, D., Ohkawa, Y., Suyama, M., and Morohashi, K.-I. (2017). Role of Ad4-binding protein/steroidogenic factor 1 in regulating NADPH production in adrenocortical Y-1 cells. Endocr. J. *64*, 315–324.

30. Baba, T., Otake, H., Inoue, M., Sato, T., Ishihara, Y., Moon, J.-Y., Tsuchiya, M., Miyabayashi, K., Ogawa, H., Shima, Y., et al. (2018). Ad4BP/SF-1 regulates cholesterol synthesis to boost the production of steroids. Commun. Biol. *1*, 18.

31. Efroni, S., Duttagupta, R., Cheng, J., Dehghani, H., Hoeppner, D.J., Dash, C., Bazett-Jones, D.P., Le Grice, S., McKay, R.D.G., Buetow, K.H., et al. (2008). Global transcription in pluripotent embryonic stem cells. Cell Stem Cell *2*, 437–447.

32. Lin, C.Y., Lovén, J., Rahl, P.B., Paranal, R.M., Burge, C.B., Bradner, J.E., Lee, T.I., and Young, R.A. (2012). Transcriptional amplification in tumor cells with elevated c-Myc. Cell *151*, 56–67.

33. Percharde, M., Wong, P., and Ramalho-Santos, M. (2017). Global Hyper-transcription in the Mouse Embryonic Germline. Cell Rep. *19*, 1987–1996.

34. Nie, Z., Hu, G., Wei, G., Cui, K., Yamane, A., Resch, W., Wang, R., Green, D.R., Tessarollo, L., Casellas, R., et al. (2012). c-Myc is a universal amplifier of expressed genes in lymphocytes and embryonic stem cells. Cell *151*, 68–79.

35. Kim, Y.-K., Cho, B., Cook, D.P., Trcka, D., Wrana, J.L., and Ramalho-Santos, M. (2023). Absolute scaling of single-cell transcriptomes identifies pervasive hypertranscription in adult stem and progenitor cells. Cell Rep. *42*, 111978.

36. Bulut-Karslioglu, A., Jin, H., Kim, Y.-K., Cho, B., Guzman-Ayala, M., Williamson, A.J.K., Hejna, M., Stötzel, M., Whetton, A.D., Song, J.S., and Ramalho-Santos, M. (2021). Chd1 protects genome integrity at promoters to sustain hypertranscription in embryonic stem cells. Nat. Commun. *12*, 4859.

37. Zubair, M., Ishihara, S., Oka, S., Okumura, K., and Morohashi, K.-I. (2006). Two-step regulation of Ad4BP/SF-1 gene transcription during fetal adrenal development: initiation by a Hox-Pbx1-Prep1 complex and maintenance via autoregulation by Ad4BP/SF-1. Mol. Cell Biol. *26*, 4111–4121.

38. Morohashi, K.-I., and Zubair, M. (2011). The fetal and adult adrenal cortex. Mol. Cell. Endocrinol. *336*, 193–197.

39. Bland, M.L., Jamieson, C.A., Akana, S.F., Bornstein, S.R., Eisenhofer, G., Dallman, M.F., and Ingraham, H.A. (2000). Haploinsufficiency of steroidogenic factor-1 in mice disrupts adrenal development leading to an impaired stress response. Proc. Natl. Acad. Sci. USA *97*, 14488–14493.

40. Miyabayashi, K., Tokunaga, K., Otake, H., Baba, T., Shima, Y., and Morohashi, K.-I. (2015). Heterogeneity of ovarian theca and interstitial gland cells in mice. PLoS One *10*, e0128352.

41. Hanukoglu, I., and Rapoport, R. (1995). Routes and regulation of NADPH production in steroidogenic mitochondria. Endocr. Res. *21*, 231–241.

42. Chambon, C., Duteil, D., Vignaud, A., Ferry, A., Messaddeq, N., Malivindi, R., Kato, S., Chambon, P., and Metzger, D. (2010). Myocytic androgen receptor controls the strength but not the mass of limb muscles. Proc. Natl. Acad. Sci. USA *107*, 14327–14332.

43. Rana, K., Chiu, M.W.S., Russell, P.K., Skinner, J.P., Lee, N.K.L., Fam, B.C., Zajac, J.D., and MacLean, H.E. (2016). Muscle-specific androgen receptor deletion shows limited actions in myoblasts but not in myofibers in different muscles in vivo. J. Mol. Endocrinol. *57*, 125–138.

44. Dubois, V., Laurent, M.R., Sinnesael, M., Cielen, N., Helsen, C., Clinckemalie, L., Spans, L., Gayan-Ramirez, G., Deldicque, L., Hespel, P., et al. (2014). A satellite cell-specific knockout of the androgen receptor reveals myostatin as a direct androgen target in skeletal muscle. FASEB J *28*, 2979–2994.

45. Hosoi, T., Yakabe, M., Sasakawa, H., Sasako, T., Ueki, K., Kato, S., Tokuoka, S.M., Oda, Y., Abe, M., Matsumoto, T., et al. (2023). Sarcopenia phenotype and impaired muscle function in male mice with fast-twitch muscle-specific knockout of the androgen receptor. Proc. Natl. Acad. Sci. USA *120*, e2218032120.

46. Sakakibara, I., Yanagihara, Y., Himori, K., Yamada, T., Sakai, H., Sawada, Y., Takahashi, H., Saeki, N., Hirakawa, H., Yokoyama, A., et al. (2021). Myofiber androgen receptor increases muscle strength mediated by a skeletal muscle splicing variant of Mylk4. iScience *24*, 102303.

47. Shimizu, N., Maruyama, T., Yoshikawa, N., Matsumiya, R., Ma, Y., Ito, N., Tasaka, Y., Kuribara-Souta, A., Miyata, K., Oike, Y., et al. (2015). A muscle-liver-fat signalling axis is essential for central control of adaptive adipose remodelling. Nat. Commun. *6*, 6693.

48. Christianto, A., Baba, T., Takahashi, F., Inui, K., Inoue, M., Suyama, M., Ono, Y., Ohkawa, Y., and Morohashi, K.-I. (2021). Sex differences in metabolic pathways are regulated by Pfkfb3 and Pdk4 expression in rodent muscle. Commun. Biol. *4*, 1264.

49. Malendowicz, L.K. (1974). Sex differences in adrenocortical structure and function. II. The effects of postpubertal gonadectomy and gonadal hormone replacement on the rat adrenal cortex evaluated by stereology at the light microscope level. Cell Tissue Res. *151*, 537–547.

50. Gritsina, G., Gao, W.-Q., and Yu, J. (2019). Transcriptional repression by androgen receptor: roles in castration-resistant prostate cancer. Asian J. Androl. *21*, 215–223.

51. Gannon, A.-L., O'Hara, L., Mason, J.I., Jørgensen, A., Frederiksen, H., Milne, L., Smith, S., Mitchell, R.T., and Smith, L.B. (2019). Androgen receptor signalling in the male adrenal facilitates X-zone regression, cell turnover and protects against adrenal degeneration during ageing. Sci. Rep. *9*, 10457.

52. Seale, J.V., Wood, S.A., Atkinson, H.C., Bate, E., Lightman, S.L., Ingram, C.D., Jessop, D.S., and Harbuz, M.S. (2004). Gonadectomy reverses the sexually diergic patterns of circadian and stress-induced hypothalamic-pituitary-adrenal axis activity in male and female rats. J. Neuroendocrinol. *16*, 516–524.

53. Raff, H., Sharma, S.T., and Nieman, L.K. (2014). Physiological basis for the etiology, diagnosis, and treatment of adrenal disorders: Cushing's syndrome, adrenal insufficiency, and congenital adrenal hyperplasia. Compr. Physiol. *4*, 739–769.

54. Gallo-Payet, N. (2016). 60 YEARS OF POMC: Adrenal and extra-adrenal functions of ACTH. J. Mol. Endocrinol. *56*, T135–T156.

55. Quinn, M.A., and Cidlowski, J.A. (2016). Endogenous hepatic glucocorticoid receptor signaling coordinates sex-biased inflammatory gene expression. FASEB J *30*, 971–982.

56. Percharde, M., Bulut-Karslioglu, A., and Ramalho-Santos, M. (2017). Hypertranscription in Development, Stem Cells, and Regeneration. Dev. Cell *40*, 9–21.

57. Morohashi, K.-I., Inoue, M., and Baba, T. (2020). Coordination of Multiple Cellular Processes by NR5A1/Nr5a1. Endocrinol. Metab. *35*, 756–764.

58. Zhang, Q., Liu, W., Zhang, H.-M., Xie, G.-Y., Miao, Y.-R., Xia, M., and Guo, A.-Y. (2020). hTFtarget: A Comprehensive Database for Regulations of Human Transcription Factors and Their Targets. Dev. Reprod. Biol. *18*, 120–128.

59. Liska, O., Bohár, B., Hidas, A., Korcsmáros, T., Papp, B., Fazekas, D., and Ari, E. (2022). TFLink: an integrated gateway to access transcription factor-target gene interactions for multiple species. Database *2022*.

60. Guo, H., Wu, Y., Nouri, M., Spisak, S., Russo, J.W., Sowalsky, A.G., Pomerantz, M.M., Wei, Z., Korthauer, K., Seo, J.-H., et al. (2021). Androgen receptor and MYC equilibration centralizes on developmental super-enhancer. Nat. Commun. *12*, 7308.

61. Mukai, T., Kusaka, M., Kawabe, K., Goto, K., Nawata, H., Fujieda, K., and Morohashi, K.-I. (2002). Sexually dimorphic expression of Dax-1 in the adrenal cortex. Gene Cell. *7*, 717–729.

62. Morohashi, K., Zanger, U.M., Honda, S., Hara, M., Waterman, M.R., and Omura, T. (1993). Activation of CYP11A and CYP11B gene promoters by the steroidogenic cell-specific transcription factor. Mol. Endocrinol. *7*, 1196–1204.

63. Sawano, S., Komiya, Y., Ichitsubo, R., Ohkawa, Y., Nakamura, M., Tatsumi, R., Ikeuchi, Y., and Mizunoya, W. (2016). A One-Step Immunostaining Method to Visualize Rodent Muscle Fiber Type within a Single Specimen. PLoS One *11*, e0166080.

64. Sasaki, G., Ishii, T., Jeyasuria, P., Jo, Y., Bahat, A., Orly, J., Hasegawa, T., and Parker, K.L. (2008). Complex role of the mitochondrial targeting signal in the function of steroidogenic acute regulatory protein revealed by bacterial artificial chromosome transgenesis in vivo. Mol. Endocrinol. *22*, 951–964.

65. Shinoda, K., Lei, H., Yoshii, H., Nomura, M., Nagano, M., Shiba, H., Sasaki, H., Osawa, Y., Ninomiya, Y., Niwa, O., et al. (1995). Developmental defects of the ventromedial hypothalamic nucleus and pituitary gonadotroph in the Ftz-F1 disrupted mice. Dev. Dyn. *204*, 22–29.

66. Andrews, S. (2010). FastQC: A Quality Control Tool for High Throughput Sequence Data. [Online]. http://www.bioinformatics.babraham.ac.uk/projects/fastqc/.

67. FastQC (2015). https://qubeshub.org/resources/fastqc.

68. Bolger, A.M., Lohse, M., and Usadel, B. (2014). Trimmomatic: a flexible trimmer for Illumina sequence data. Bioinformatics *30*, 2114–2120.

69. Dobin, A., Davis, C.A., Schlesinger, F., Drenkow, J., Zaleski, C., Jha, S., Batut, P., Chaisson, M., and Gingeras, T.R. (2013). STAR: ultrafast universal RNA-seq aligner. Bioinformatics *29*, 15–21.

70. Liao, Y., Smyth, G.K., and Shi, W. (2014). featureCounts: an efficient general purpose program for assigning sequence reads to genomic features. Bioinformatics *30*, 923–930.

71. Love, M.I., Huber, W., and Anders, S. (2014). Moderated estimation of fold change and dispersion for RNA-seq data with DESeq2. Genome Biol. *15*, 550.

72. Kent, W.J., Sugnet, C.W., Furey, T.S., Roskin, K.M., Pringle, T.H., Zahler, A.M., and Haussler, D. (2002). The human genome browser at UCSC. Genome Res. *12*, 996–1006.

73. Huang, D.W., Sherman, B.T., and Lempicki, R.A. (2009). Systematic and integrative analysis of large gene lists using DAVID bioinformatics resources. Nat. Protoc. *4*, 44–57.

74. Langmead, B., and Salzberg, S.L. (2012). Fast gapped-read alignment with Bowtie 2. Nat. Methods *9*, 357–359.

75. Li, H., Handsaker, B., Wysoker, A., Fennell, T., Ruan, J., Homer, N., Marth, G., Abecasis, G., and Durbin, R.; 1000 Genome Project Data Processing Subgroup (2009). Genome Project Data Processing Subgroup (2009). The Sequence Alignment/Map format and SAMtools. Bioinformatics *25*, 2078–2079.

76. Zhang, Y., Liu, T., Meyer, C.A., Eeckhoute, J., Johnson, D.S., Bernstein, B.E., Nusbaum, C., Myers, R.M., Brown, M., Li, W., and Liu, X.S. (2008). Model-based analysis of ChIP-Seq (MACS). Genome Biol. *9*, R137.

77. Quinlan, A.R., and Hall, I.M. (2010). BEDTools: a flexible suite of utilities for comparing genomic features. Bioinformatics *26*, 841–842.

78. Bailey, T.L., Johnson, J., Grant, C.E., and Noble, W.S. (2015). The MEME Suite. Nucleic Acids Res. *43*, W39–W49.

79. Yu, G., Wang, L.-G., and He, Q.-Y. (2015). ChIPseeker: an R/Bioconductor package for ChIP peak annotation, comparison and visualization. Bioinformatics *31*, 2382–2383.

80. Wang, Q., Li, M., Wu, T., Zhan, L., Li, L., Chen, M., Xie, W., Xie, Z., Hu, E., Xu, S., and Yu, G. (2022). Exploring Epigenomic Datasets by ChIPseeker. Curr. Protoc. *2*, e585.

81. Robinson, J.T., Thorvaldsdóttir, H., Winckler, W., Guttman, M., Lander, E.S., Getz, G., and Mesirov, J.P. (2011). Integrative genomics viewer. Nat. Biotechnol. *29*, 24–26.

82. Schindelin, J., Arganda-Carreras, I., Frise, E., Kaynig, V., Longair, M., Pietzsch, T., Preibisch, S., Rueden, C., Saalfeld, S., Schmid, B., et al. (2012). Fiji: an open-source platform for biological-image analysis. Nat. Methods *9*, 676–682.

83. Wickham, H. (2016). ggplot2: Elegant Graphics for Data Analysis (Springer-Verlag). https://ggplot2.tidyverse.org.

84. Ihaka, R., and Gentleman, R. (1996). R: a language for data analysis and graphics. J. Comput. Graph Stat. *5*, 299–314. http://www.R-project.org.

85. External RNA Controls Consortium (2005). Proposed methods for testing and selecting the ERCC external RNA controls. BMC Genom. *6*, 150.

86. Jao, C.Y., and Salic, A. (2008). Exploring RNA transcription and turnover *in vivo* by using click chemistry. Proc. Natl. Acad. Sci. USA *105*, 15779–15784.

87. Sherman, B.T., Hao, M., Qiu, J., Jiao, X., Baseler, M.W., Lane, H.C., Imamichi, T., and Chang, W. (2022). DAVID: a web server for functional enrichment analysis and functional annotation of gene lists (2021 update). Nucleic Acids Res. *50*, W216–W221.

88. Larsson, C.A., Gullberg, B., Råstam, L., and Lindblad, U. (2009). Salivary cortisol differs with age and sex and shows inverse associations with WHR in Swedish women: a cross-sectional study. BMC Endocr. Disord. *9*, 16.

89. Skene, P.J., and Henikoff, S. (2017). An efficient targeted nuclease strategy for high-resolution mapping of DNA binding sites. Elife *6*, e21856.

90. Amemiya, H.M., Kundaje, A., and Boyle, A.P. (2019). The ENCODE Blacklist: Identification of Problematic Regions of the Genome. Sci. Rep. *9*, 9354.

91. Bailey, T.L., and Machanick, P. (2012). Inferring direct DNA binding from ChIP-seq. Nucleic Acids Res. *40*, e128.

STAR★METHODS

KEY RESOURCES TABLE

REAGENT or RESOURCE	SOURCE	IDENTIFIER
Antibodies		
Rabbit polyclonal anti-Ad4BP/SF-1	Morohashi et al.[62]	N/A
Rabbit polyclonal anti-Histone H3	Invitrogen	PA5-16183; RRID: AB_10985434
Rabbit IgG	ZYMED Laboratories	02-6102; RRID: AB_2532938
Anti-Rabbit IgG, HRP-Linked F(ab')$_2$ Fragment Donkey	GE Healthcare	NA9340V; RRID: AB_772206
Rat monoclonal anti-MyHC2B	Sawano et al.[63]	N/A
Rabbit polyclonal anti-laminin	Sigma	L9393; RRID: AB_477163
Mouse Anti-Rat IgG2b-AF647 (2B10A8)	SouthernBiotech	Cat# 3070-3; RRID: AB_2795888
Alexa Fluor 488-labeled Goat Anti-Rabbit IgG	Invitrogen	A11008; RRID: AB_143165
Chemicals, peptides, and recombinant proteins		
5α-Dihydrotestosterone	Wako	045–26071
β-Estradiol	Sigma	E8875
Flutamide	Sigma	F9397
Corn oil	Nacalai Tesque	25606–65
SEROTROPIN® for animal (PMSG)	ASKA Pharmaceutical	N/A
GONATROPIN®3000 for animal (hGC)	ASKA Pharmaceutical	N/A
Ribonuclease A	Nacalai Tesque	30100–31
Collagenase	Sigma	C0130
Trypsin inhibitor	Sigma	T9003
DNase I	Roche	11284932001
5-Ethynyluridine	BLD Pharmatech	69075-42-9
Azide-fluor 545	Sigma	760757
7-AAD	BD Bioscience	51-68981E
XF DMEM Medium, pH 7.4	Agilent	Part# 103575-100
Cell-Tak	Corning	354240
9,11,12,12-d_4-corticosterone	IsoSciences	Cas: 50-22-6
Corticosterone-9,11,12,12-d_4	Sigma	802905
testosterone (2,3,4-$^{13}C_3$, 99%)	Cambridge Isotope Laboratories	58-22-0
Estradiol (2,4,16,16-d_4)	Cambridge Isotope Laboratories	57-63-6
Protease Inhibitor Cocktail for Use with Mammalian Cell and Tissue Extracts	Nacalai Tesque	25955–11
Digitonin	Millipore	300410-1GM
pAG/MNase	addgene	123461
4′, 6' -diamidino-2-phenylindole (DAPI)	Sigma	D8417
Critical commercial assays		
Qubit dsDNA HS Assay Kit	invitrogen	Q32851
ERCC RNA Spike-In Control Mix	invitrogen	4456740
RNeasy Micro kit	Qiagen	Cat# 74004
Agilent RNA 6000 pico Kit	Agilent	5067–1513
NEBNext Poly(A) mRNA Magnetic Isolation Module	New England Biolabs	E7490
NEBNext Ultra II RNA Directional Library Prep with Sample Purification Beads	New England Biolabs	E7765
NEBNext Ultra II DNA Library Prep Kit	New England Biolabs	E7645

(*Continued on next page*)

Continued

REAGENT or RESOURCE	SOURCE	IDENTIFIER
NEBNext Multiplex Oligos for Illumina (96 Unique Dual Index Primer Pairs)	New England Biolabs	E6440
AMPure XP Reagent, 60 mL	BECKMAN COULTER	A63881
Seahorse XF Cell Glycolysis Stress Test Kit	Agilent	Cat# 103020-100
Seahorse XF Cell Mito Stress Test Kit	Agilent	Cat# 103015-100
Seahorse XFe96 FluxPaks	Agilent	Cat#102416-100
SYBR Select Master Mix	Applied Biosystems	4472897
Chemi-Lumi One L	Nacalai Tesque	07880–70
BioMag®Plus Concanavalin A	Polysciences	Cat# 86057-3
CellTiter-Glo Luminescent Cell Viability Assay	Promega	G7571
NADP/NADPH Assay Kit-WST	DOJINDO	N510
Deposited data		
CNN RNA-seq dataset	This paper	DDBJ: DRA015952, DRA017476
CUT&RUN-seq dataset	This paper	DDBJ: DRA015953, DRA017475
Original blots	This paper	Mendeley Data: https://doi.org/10.17632/sw84wbvnzd.2
FastQC data of CUT&RUN-seq	This paper	Mendeley Data: https://doi.org/10.17632/sw84wbvnzd.2
Experimental models: Organisms/strains		
Mouse: Ad4BP-BAC-EGFP	Miyabayashi et al.[40]	N/A
Mouse: StAR-EGFP	Sasaki et al.[64]	N/A
Mouse: *Nr5a1*$^{+/-}$	Shinoda et al.[65]	N/A
Mouse: C57BL/6J	Japan SLC	C57BL/6JJmsSlc
Oligonucleotides		
See Table S6 for all oligos and primers.		
Software and algorithms		
FastQC v0.11.9	Brown et al.[66,67]	RRID:SCR_014583
Trimmomatic v0.39	Bolger et al.[68]	RRID:SCR_011848
STAR v2.7.0a	Dobin et al.[69]	RRID:SCR_004463
featureCounts v1.6.4	Liao et al.[70]	RRID:SCR_012919
DESeq2 v1.36.0	Love et al.[71]	RRID:SCR_015687
DAVID	Huang et al.[72,73]	RRID:SCR_001881
Bowtie2 v2.4.4	Langmead et al.[74]	RRID:SCR_016368
SamTools v0.3.3	Li et al.[75]	RRID:SCR_002105
MACS2 v2.2.7.1	Zhang et al.[76]	RRID:SCR_013291
bedtools v2.30.0	Quinlan et al.[77]	RRID:SCR_006646
MEME Suite v5.5.0	Bailey et al.[78]	RRID:SCR_001783
ChIPseeker v3.16	Yu et al.[79,80]	RRID:SCR_021322
Igv	Robinson et al.[81]	RRID:SCR_011793
Fiji	Schindelin et al.[82]	RRID:SCR_002285
ggplot2 v3.4.0	Wickman[83]	RRID:SCR_014601
R v4.2.3	Ihaka et al.[84]	RRID:SCR_001905
AppSan	Bay bioscience	N/A
Zen blue 3.5	Zeiss	RRID:SCR_013672
Other		
NanoDrop ND-1000	Thermo Fisher Scientific	N/A
QubitR3.0 Fluorometer	Life technologies	N/A
JSAN	Bay bioscience	N/A
Countess II FL	Thermo Fisher Scientific	N/A
Agilent 2100 Bioanalyzer	Agilent	N/A
Seahorse XFe96 Analyzer	Agilent	N/A

(*Continued on next page*)

Continued

REAGENT or RESOURCE	SOURCE	IDENTIFIER
GC 2010 Plus gas chromatography	Shimadzu	N/A
triple-quadrupole GCMS-TQ8050	Shimadzu	N/A
ACQUITY UPLC™ BEH C18 column	Waters	186002350
ACQUITY UPLC™ BEH C18 VanGuard™ Pre-column	Waters	186003975
Xevo™ TQ-S micro triple quadrupole mass spectrometry system	Waters	N/A
Bioruptor UCD-300	Cosmo Bio	N/A
ImageQuant LAS 500	GE healthcare	N/A
EnSight	PerkinElmer	N/A
iMark	Bio-Rad	N/A
LSM700 confocal laser scanning microscope	Zeiss	N/A

RESOURCES AVAILABILITY

Lead contact

Requests for further information, resources, and reagents should be directed to and will be fulfilled by the lead contact, Ken-ichirou Morohashi (morohashi.ken-ichirou.874@m.kyushu-u.ac.jp).

Materials availability

This study did not generate new unique materials.

Data and code availability

- CNN RNA-seq and CUT&RUN-seq data have been deposited in DDBJ (DNA DataBank of Japan) and are publicly available under the following accession numbers: DDBJ: DRA015952, DRA017476, DRA015953, and DRA017475. A PDF file with uncropped western blot images has been deposited in Mendeley Data and is publicly available under the following site: Mendeley Data: https://doi.org/10.17632/sw84wbvnzd.2.
- This paper does not report the original code.
- Any additional information required to reanalyze the data reported in this paper is available from the lead contact upon request.

EXPERIMENTAL MODEL AND SUBJECT DETAILS

Mice

Two transgenic mouse lines, *Ad4BP-BAC-EGFP*[40] and *StAR-EGFP*,[64] whose adrenocortical cells are labeled with EGFP, were used to obtain zF cells and sera. By crossing *Ad4BP-BAC-EGFP* and heterozygotes of *Nr5a1* (*Nr5a1*$^{+/-}$),[65] we obtained EGFP-labeled zF cells from wild-type and *Nr5a1*$^{+/-}$ offspring. *Nr5a1*$^{+/-}$ mice were also crossed with C57BL/6J mice to obtain skeletal muscles from wild-type and *Nr5a1*$^{+/-}$ offspring. All mice were fed with standard CRF-1 chow (Oriental Yeast, Tokyo, Japan) and housed in a controlled environment with 12-h light-dark cycle (lights on: 8 a.m. to 8 p.m.). Unless expressly stated, the mice were sacrificed in the morning (8–10 a.m.). All protocols for the animal experiments were approved by the Animal Care and Use Committee of Kyushu University. All experiments were performed in accordance with institutional guidelines.

METHOD DETAILS

Sex steroids treatment

Mice were gonadectomized or sham-operated at 3 weeks after birth. Two weeks after the operation, 100 μL DHT (5α-Dihydrotestosterone, 50 μg/mL in 5% ethanol in corn oil, Wako, Osaka, Japan) was injected subcutaneously once every day for three weeks, while 100 μL E2 (β-Estradiol, 5 μg/mL in 5% ethanol in corn oil, Sigma, St. Louis, MO) was injected at 47, 51, and 55 days after birth. The adrenal glands were prepared from these mice at 8 weeks. For females, 0.2 mL of PMSG (pregnant mare serum gonadotropin, 37.5 units/mL in saline, ASKA Pharmaceutical, Tokyo, Japan) and 0.2 mL of hCG (human chorionic gonadotropin, 37.5 units/mL in saline, ASKA Pharmaceutical) were intraperitoneally injected at 5 p.m. of 53 and 55 days, respectively, to excite superovulation. The mice after 4 and 48 h of the hCG treatment were utilized as the mice corresponding to estrus and diestrus females, respectively. Every experimental group comprised three male or three female mice, and they were kept in a single cage.

Flutamide treatment

Mice were subcutaneously injected with 100 μL flutamide (400 μg/mL in corn oil, Sigma) or with 100 μL corn oil as a control once every day. The daily flutamide or corn oil injection began 74 days after birth (Figure S2H). Adrenals were prepared from these mice at 12 weeks. For females, we checked their vaginal smear and only mice at a diestrus stage were used for the study.

Preparation of zF cells

The adrenals from 8-week-old *Ad4BP-BAC-EGFP* or *StAR-EGFP* transgenic mice were used. Adrenocortical tissues corresponding to zF were collected under microscopic observation using micro scissors. The tissues were dispersed with HBSS (Hank's balanced salt solution) supplemented with 1 mM $MgCl_2$, 5 mg/mL BSA (bovine serum albumin), 1 mg/mL collagenase (Sigma), 0.25 mg/mL trypsin inhibitor (Sigma), and 0.5 mg/mL DNase I (Roche, Basel, Switzerland) for 1 h at 37°C. The dispersed cells were filtered through a 35 μm cell strainer, followed by centrifugation at 300*g* for 5 min and re-suspended in DMEM/F12 medium supplemented with 2% BSA and 1 mM EDTA. The resultant cells were stained with 7-AAD (7-aminoactinomycin D, BD Bioscience, Franklin Lakes, NJ), followed by FACS using JSAN (Bay bioscience, Hyogo, Japan) to sort alive zF cells based on 7-AAD and EGFP fluorescence; the zF cells were prepared as $7\text{-AAD}^-/\text{EGFP}^+$. The number of zF cells was counted using Countess II FL (Thermo Fisher Scientific). RT-PCR was performed to confirm that the prepared cells did not contain any other adrenal cells than zF cells using primers specific for marker genes expressing in zona glomerulosa, X-zone, and medulla (Table S4).

Quantification of total RNA and mRNA prepared from zF tissue

The adrenals from 8-week-old Ad4BP-BAC-EGFP mice were used. Adrenocortical tissues corresponding to zF were lysed into lysis buffer (50 mM Tris-HCl (pH 8.0), 50 mM NaCl, 1 mM EDTA, and 1% SDS) and were equally split into two aliquots for total RNA and genome DNA extraction. Total RNA was extracted using an RNeasy Micro kit (QIAGEN, Hilden, Germany) from an aliquot. Another aliquot was treated with Ribonuclease A (Nacalai Tesque, Kyoto, Japan) at 37°C for 30 min and then DNA was obtained by Phenol/Chloroform/Isoamyl Alcohol extraction followed by ethanol precipitation. mRNA was isolated from 1 μg Total RNA using NEBNext Poly(A) mRNA Magnetic Isolation Module (New England Biolabs, Ipswich, MA). The amount of Total RNA and mRNA were quantified by NanoDrop (Thermo Fisher Scientific, Waltham, MA). The amount of genomic DNA was quantified by Qubit (Life Technologies, Carlsbad, CA). The amounts of total RNA and mRNA per unit cell-number were calculated as follows. Firstly, we quantified the amounts of total RNA and genomic DNA prepared from the aliquots and calculated the total RNA amount per 1 μg of genomic DNA (total RNA amount/μg genomic DNA). This value corresponds to the total RNA amount corrected for cell number. Subsequently, mRNA was isolated from 1 μg of total RNA. By quantifying the purified mRNA amount, we calculated the amount of mRNA contained in 1 μg of total RNA (mRNA amount/μg total RNA). Finally, by multiplying the "total RNA amount per 1 μg of genomic DNA" and "the amount of mRNA in 1 μg of total RNA," the mRNA amount in 1 μg of genomic DNA was determined.

Preparation of total RNA and mRNA from zF cells

Total RNA was isolated from 10,000 zF cells of male and female *Ad4BP-BAC-EGFP* mice using an RNeasy Micro Kit. RNA integrity numbers were confirmed to be higher than 8 using an Agilent RNA 6000 pico Kit with Agilent 2100 Bioanalyzer (Agilent, Santa Clara, CA). Four microliters of 10,000-fold diluted ERCC (External RNA Controls Consortium) control mix (Invitrogen, Waltham, MA)[85] was added to the total RNA. Poly(A) RNA was prepared from the total RNA using the NEBNext Poly(A) mRNA Magnetic Isolation Module.

Nascent transcription assay

The adrenals from 8-week-old Ad4BP-BAC-EGFP transgenic mice were used. zF tissues were dispersed as described above. After the dispersed zF cells were washed twice in incubation buffer (D-MEM (Nacalai Tesque) supplemented with 10% FBS-charcoal stripped (Serana Europe GmbH, Brandenburg, Germany)), they were incubated to label nascent RNA with 1 mM 5-ethynyl-uridine (EU, BLD pharmatech, Shanghai, China) at 37°C for 1 h in the incubation buffer. The cells were filtered through a 35 μm cell strainer, followed by washing with PBS twice, and finally recovered by centrifugation at 300*g* for 5 min. Nascent RNA labeled with EU was detected with the method described previously.[86] Briefly, cells were fixed with 0.5% formalin for 30 min in PBS supplemented with 0.03% Triton X-100. The fixed cells were washed twice in PBS supplemented with 0.03% Triton X-100 and incubated for 30 min with 25 μM Azide-fluor 545 (red fluorescein, Sigma) to label the EU incorporated RNAs in 100 mM Tris-HCl (pH 8.5) supplemented with 1 mM $CuSO_4$ and 100 mM ascorbic acid. After the cells were washed twice and resuspended with PBS, they were analyzed using JSAN. The number and the red-fluorescence intensity of EGFP positive cells (zF cells) were quantified by flow cytometry.

CNN RNA-seq and data processing

Transcriptome datasets were obtained by CNN RNA-seq.[33] Briefly, Libraries for RNA-seq were constructed using NEBNext Ultra II Directional RNA Library Prep Kit for Illumina (New England Biolabs) and NEBNext Multiplex Oligos for Illumina (96 Unique Dual Index Primer Pairs, New England Biolabs) and then sequenced using HiSeq 2500 (151-bp paired-end, Illumina). Paired-end read tags those passed quality control by FastQC[66,67] and Trimmomatic[68] were mapped to the reference genome (mm10) utilizing STAR (Spliced transcripts Alignment to a Reference).[69] Read-annotation and count were computed using featureCounts (option "-M, -O, -p").[70] Mean values for biological replicates (n = 3) were calculated, and genes with mean count values >300 were identified as expressed genes. The absolute scaling of ERCC datasets was performed using DESeq2.[71] This scaling was derived from the sum of all ERCC

spike-in reads and calculates a set of size factors. Expression values of each gene were then normalized to the size factors. Reference sequence of mice genome (mm10) and gene annotation files were downloaded from the UCSC Genome Browser[72] and were modified by integrating EGFP and ERCC sequences. Gene expression data are presented as normalized counts. Differentially expressed genes were subjected to KEGG pathway enrichment analysis using DAVID.[73,87]

Measurement of ECAR and OCR

zF cells were seeded onto Cell-Tak pre-coated XF96 cell culture microplates (15,000 cells/well) (Agilent). ECAR (ExtraCellular Acidification Rate) was measured with Seahorse XFe96 Analyzer (Agilent). After basal measurements, 10 mM glucose, 0.5 μM rotenone/antimycin A, and 50 mM 2-deoxy-D-glucose (2-DG) were sequentially injected. All reagents were provided in a Seahorse XF Glycolytic Stress Test Kit (Agilent). OCR (Oxygen Consumption Rate) was also measured with the analyzer. After basal measurements, 1.5 μM oligomycin, 0.5 μM FCCP (Carbonyl cyanide 4-(trifluoromethoxy)phenylhydrazone), and 0.5 μM rotenone/antimycin A were sequentially injected. All reagents were provided in a Seahorse XF Cell Mito Stress Test Kit (Agilent).

Measurement of serum steroids

Sera were collected by cardiac puncture from 8 to 12 weeks old mice at 6 p.m. for corticosterone and at 8 p.m. for testosterone measurement. Anesthesia was not performed because anesthetics is known to increase corticosterone levels.[88] Serum collection was completed within approximately 15 s from the time of handling of mice. Collected sera were stored at −30°C until use. Corticosterone-9,11,12,12-d_4 (Sigma), and testosterone (2,3,4-$^{13}C_3$, 99%) (Cambridge Isotope Laboratories, Inc., USA) were used as internal standards. Lipids were extracted from 20 μL of the sera using the method of Bligh and Dyer with the internal standards. The organic phase was transferred to a clean vial and dried under a nitrogen stream. The lipid extracts were then derivatized with 100 μL of Girard's reagent T (5 mg/mL in MeOH containing 0.1% trifluoroacetic acid) at 37°C for 60 min, and the reaction was stopped with 100 μL of methanol with 0.028% NH_4OH. 1 μL of the derivatized lipids was injected onto an ultra-high-performance liquid chromatography (UHPLC)–electrospray ionization (ESI)–tandem mass spectrometry (MS/MS) system. LC separation was performed on an ACQUITY UPLC BEH C18 column (1.7 μm, 2.1 × 50 mm; Waters, Milford, MA, USA) coupled to an ACQUITY UPLC BEH C18 VanGuard Pre-column (1.7 μm, 2.1 × 5 mm; Waters). Mobile phase A was H_2O containing 0.1% (v/v) formic acid, and mobile phase B was acetonitrile containing 0.1% (v/v) formic acid. The LC gradient consisted of a linear gradient from 95% A to 100% B over 12 min, 100% B for 5 min, and equilibration with 95% A for 5 min (22 min total run time). The flow rate was 0.3 mL/min and the column temperature was 25°C. Multiple reaction monitoring (MRM) was performed in the positive ion mode using a Xevo TQ-S micro triple quadrupole mass spectrometry system (Waters) equipped with an ESI source. The ESI capillary voltage was set at 1.0 kV, and the sampling cone was set at 30 V. The source temperature was 150°C, the desolvation temperature was 500°C, and the desolvation gas flow was 1000 L/h. The cone gas flow was 50 L/h.

Sera were collected by cardiac puncture from 12-week-old female mice for E2 measurement. The female mice were treated with PMSG and hCG as described above. 4 h after hCG injection, sera were recovered from the mice. Estradiol (2,4,16,16-d_4) (Cambridge Isotope Laboratories, Inc., USA) was used as an internal standard. About 50 μL of the sera and the internal standard were transferred to 1.5-mL polypropylene tubes and diluted with water to 100 μL. The samples were vortexed with 200 μL of acetonitrile for 30–60 s for protein precipitation. Then, 1 mL of methyl *tert*-butyl ether was added to the tubes, followed by vortexing for 30–60 s. After centrifugation at 13,000 × g for 5 min at room temperature, the organic (upper) phase was transferred to clean 1.5-mL polypropylene tubes and dried under a nitrogen stream at 50°C. The dried residue was redissolved with 50 μL of sodium bicarbonate buffer (0.1 mM, pH10.5), and derivatized with 50 μL of dansyl chloride (1 mg/mL in acetonitrile) at 60°C for 10 min. After centrifugation at 13,000 × g for 5 min at room temperature to remove insoluble residues, 10 μL of the supernatant was injected onto a UHPLC–ESI–MS/MS system. LC separation was performed on a CORTECS UPLC C18 column (1.6 μm, 2.1 × 100 mm; Waters) coupled to an CORTECS UPLC C18 VanGuard Pre-column (1.6 μm, 2.1 × 5 mm; Waters). Mobile phase A was H_2O containing 0.1% (v/v) formic acid, and mobile phase B was acetonitrile containing 0.1% (v/v) formic acid. The LC gradient consisted of a linear gradient from 95% A to 70% B over 6 min, a linear gradient to 100% B over 9 min, 100% B for 5 min, and equilibration with 95% A for 5 min (25 min total run time). The flow rate was 0.35 mL/min, and the column temperature was 45°C. MRM was performed in the positive ion mode using a Xevo TQ-S micro triple quadrupole mass spectrometry system (Waters) equipped with an ESI source. The ESI capillary voltage was set at 1.0 kV, and the sampling cone was set at 30 V. The source temperature was 150°C, the desolvation temperature was 500°C, and the desolvation gas flow was 1000 L/h. The cone gas flow was 50 L/h.

CNN qRT-PCR

Similar to CNN RNA-seq, 10,000 zF cells of male and female Ad4BP-BAC-EGFP mice were lysed in Buffer RLT. Total RNA was prepared from the cells using an RNeasy Micro Kit and used to generate cDNA. The primers used for the CNN qRT-PCR are listed in Table S6. Since any normalization based on concentration of total RNA or on expression level of endogenous control genes was not performed, the CNN qRT-PCR data provides the amount of target mRNA in 10,000 zF cells.

Immunoblotting

Cell lysates were prepared from 10,000 zF cells using lysis buffer (50 mM Tris-HCl (pH 8.0), 50 mM NaCl, 1 mM EDTA, 1% SDS, Protease Inhibitor Cocktail (Nacalai Tesque)), and were treated with Bioruptor (Cosmo Bio, Tokyo, Japan) to disrupt cellular DNA. The cell

lysates were subjected to SDS polyacrylamide gel electrophoresis, followed by immunoblotting. Antibodies against NR5A1 (1:1,000, Morohashi et al.[62]) and pan Histone H3 (1:3,000, Invitrogen) were used as the primary antibodies, while HRP-Linked donkey anti-Rabbit IgG (1:5,000, GE Healthcare, Chicago, IL) was used as the secondary antibody. A chemiluminescence developed by Chemi-Lumi One L (Nacalai Tesque) was observed using LAS500 (GE Healthcare).

CUT&RUN-seq and data processing

CUT&RUN (Cleavage Under Target & Release Using Nuclease) for NR5A1 and following library preparation were independently performed with biological duplicates. CUT&RUN was performed as described.[89] Briefly, the 50,000 zF cells of male and female StAR-EGFP mice bound to Concanavalin A beads (Polyscience, Warrington, PA) were permeabilized with 0.02% digitonin at room temperature for 10 min, and incubated with anti-NR5A1 antibody (1 μg/μL) or normal rabbit IgG (1 μg/μL, ZYMED Laboratories, South San Francisco, CA) overnight at 4°C on a rotator. Then, 150 μL of pAG/MNase (700 ng/mL) was added to the sample, and digestion was allowed to proceed for 30 min at 4°C. After the digestion, samples were incubated for 10 min at 37°C to release DNA of CUT&RUN fragments. The DNA was purified by phenol/chloroform extraction followed by ethanol precipitation. The purified CUT&RUN fragments were subjected to library construction using NEBNext Ultra II DNA Library Prep Kit (New England Biolabs) and NEBNext Multiplex Oligos for Illumina (96 Unique Dual Index Primer Pairs, New England Biolabs), and then the libraries were sequenced using NextSeq (151-bp paired-end; Illumina). The paired-end reads were quality-controlled using FastQC and Trimmomatic. Then the reads were mapped to the reference mouse genome (mm10) by Bowtie2.[74] Reference genome and gene annotation files (mm10) were downloaded from the UCSC Genome Browser. Using SamTools,[75] the mapped reads were down-sampled to 20 million to fairly compare between samples. Reads mapped to the Blacklist regions[90] were eliminated. NR5A1 peaks called with MACS2[76] using the reads from normal rabbit IgG CUT&RUN data as background were divided into two classes, common (peaks are overlapped between male and female even at 1 bp) and sex-specific (peaks do not show any overlap between male and female) using bedtools.[77] The motif extraction was conducted using the Multiple Em for Motif Extraction Suite.[78] The option '-maxk', which specifies the maximum width of the motif core, was set to 9 according to the previously identified consensus binding motif of NR5A1.[17] Maximum central enrichment in a set of the CUT&RUN-seq peak regions was predicted and the positional distributions of the regions were displayed by CentriMo.[91] Read counts on each peak were computed using featureCounts. All peaks were categorized into upstream (<10 kb upstream from the transcription initiation site), intragenic, downstream (<10 kb downstream of the transcription termination site), and intergenic by using ChIPseeker.[79,80] Peaks located at upstream, intragenic, or downstream were tied to the nearest genes. Peaks were visualized by igv genome browser.[81]

Quantification of cellular ATP and NADPH

Cellular amounts of ATP and NADPH were measured using CellTiter-Glo (Promega, Madison, WI) and NADP/NADPH assay Kits (DOJINDO, Tokyo, Japan), respectively. Briefly, cell lysates were prepared from 10,000 zF cells using lysis buffers provided in the kits. Then the lysates were mixed with the reaction buffers also provided in the kits. The reacted solutions were subjected to multi-mode plate reader EnSight (PerkinElmer, Waltham, MA) and micro plate reader iMark (Bio-Rad, Hercules, CA) to determine ATP and NADPH amounts, respectively.

Measurement of muscles fiber CSA (cross sectional area)

Cryosections of the muscles (gastrocnemius, quadriceps, and triceps) of four experimental groups (wild-type female, *Nr5a1*$^{+/-}$ female, wild-type male, and *Nr5a1*$^{+/-}$ male) were subjected to immunofluorescence as previously described.[48] In brief, antibodies against MYH4 (1:1,000, Sawano et al.[63]) and laminin (1:1,000, Sigma) were used as the primary antibodies, while mouse anti–rat IgG2b-Alexa Fluor 647 (1:500, SouthernBiotech, Birmingham, AL) and Alexa Fluor 488–labeled goat anti–rabbit IgG (1:500, Invitrogen) were used as the secondary antibodies. Nuclei were stained with DAPI (4′,6-diamidino-2-phenylindole, Sigma). Fluorescence was observed using an LSM700 confocal laser scanning microscope (Zeiss, Oberkochen, Germany). Images were analyzed using Fiji software[82] to determine the CSAs of the type IIb muscle fibers. The mean number of fibers analyzed in wild-type females, *Nr5a1*$^{+/-}$ females, wild-type males, and *Nr5a1*$^{+/-}$ males are presented in corresponding order for each muscle as follows: for gastrocnemius, 6,200, 5,000, 6,000, and 5,000 fibers, respectively; for quadriceps, 4,400, 4,400, 4,300, and 4,600 fibers, respectively; for triceps, 2,900, 3,400, 3,400, and 4,600 fibers, respectively.

QUANTIFICATION AND STATISTICAL ANALYSIS

Parametric tests were conducted using unpaired two-tailed Student's t test for two groups or one-way analysis of variance (ANOVA) with Bonferroni multiple comparison test for more than two groups. When data were not normally distributed, non-parametric tests were used (Mann-Whitney's U test for two groups, Kruskal-Wallis with Dunn's multiple comparison test for more than two groups). Statistics information can be found in the figure legends.